Studies in Biomimetic Diiron(III) Chemistry and
Zeolite-Encapsulated Iron Complexes

by

Kevin L. Ward

B.A., Chemistry

Williams College, 1993

Submitted to the Department of Chemistry
in Partial Fulfillment of the Requirements for the Degree of
Master of Science in Chemistry

at the

Massachusetts Institute of Technology

June 1996

Signature of Author _____

Department of Chemistry
May 31, 1996

Certified by _____

Stephen J. Lippard
Arthur Amos Noyes Professor of Chemistry
Thesis Supervisor

Accepted by ____

Dietmar Seyferth
Chairman, Departmental Committee on Graduate Students

Science

STUDIES IN BIOMIMETIC DIIRON(III) CHEMISTRY AND

ZEOLITE-ENCAPSULATED IRON COMPLEXES

by

KEVIN L. WARD

Submitted to the Department of Chemistry
on May 31, 1996 in partial fulfillment of the
requirements for the Degree of Master of Science
in Chemistry

ABSTRACT

This thesis is concerned with two different approaches to modeling the chemistry of dinuclear non-heme iron proteins. The first involves the preparation of small model complexes which closely mimic the active site structures of hemerythrin, methane monooxygenase, or ribonucleotide reductase. The second approach is to encapsulate iron complexes inside a zeolite as a way of imitating the effect of the protein framework, which prevents the bimolecular decomposition of oxidizing intermediates.

Several carboxylate-bridged (μ-oxo)diiron(III) complexes were prepared and spectroscopically characterized. A compound with five nitrogen donor atoms as ligands and one labile coordination site, [Fe$_2$O(XDK)(BIPhMe)(tacn)(H$_2$O)](NO$_3$)$_2$ (5), was designed as an accurate structural model for the active site of hemerythrin. This complex reacts with one equivalent of azide to give a product with spectroscopic characteristics remarkably similar to those of azidomethemerythrin. In addition, it catalyzes the disproportionation of hydrogen peroxide, a process which may involve a step analogous to dioxygen release from hemerythrin. The X-ray crystal structures of a DMSO solvento complex, [Fe$_2$O(XDK)(DMSO)$_6$](NO$_3$)$_2$ (3), and an unusual hydroxide-bridged diiron(III) compound, [Fe$_2$(OH)(XDK)(BIPhMe)(H$_2$O)(NO$_3$)$_3$] (4), are also presented.

High-silica faujasites impregnated with several nitrogen donor ligands have been prepared and characterized by solid state CPMAS-NMR. Addition of Fe^{2+} to

at least one of these materials, HPTP-FAU, appears to result in the formation of an intrazeolitic diiron(II) complex. Only a small amount of Fe^{2+} can be loaded into the faujasite, whether or not an organic ligand is present. These Fe-containing faujasites are slow catalysts for the oxidation of cylcohexene with H_2O_2. The major product is the epoxide, with lesser amounts of allylic oxidation products being produced. Since this activity does not require a ligand, the catalytic species is most likely an iron atom associated with the lattice of the faujasite.

Thesis Supervisor: Stephen J. Lippard

Title: Arthur Amos Noyes Professor of Chemistry

TABLE OF CONTENTS

LIST OF TABLES

5

LIST OF FIGURES

6

ACKNOWLEDGEMENTS

Chapter 1

Modeling Dinuclear Non-Heme Iron Centers

Proteins and enzymes with dinuclear non-heme iron in their active sites carry out a variety of functions in biology. Hemerythrin (Hr) is a dioxygen transport protein,[1] the hydroxylase of soluble methane monooxygenase (sMMO) converts alkanes to alcohols,[2] and the R2 protein of ribonucleotide reductase (RNR) generates a stable tyrosyl radical.[3] All of these functions involve the reaction of dioxygen with a diiron(II) carboxylate-bridged core, but the differences among the proteins lead to different results. Understanding what features of these proteins account for their various reactivities is of significant interest, and building chemical models of the active sites helps a great deal in elucidating the chemistry of the carboxylate-bridged diiron structural motif. In particular, functional models are desirable as a way of identifying which features are necessary and sufficient for activity, and also because functional models of low molecular weight may be useful for a number of applications.

One approach to producing functional models is to mimic the coordination environment found in the protein as closely as possible. Nature has optimized the structures of these active sites for their particular functions over millions of years, so it is reasonable to think that there is something unique about the donor sets and ligand geometries found in the proteins. There have been a number of structural models for the oxo-bridged, bis(carboxylate) diiron(III) core found in methemerythrin and the oxidized forms of other non-heme diiron proteins,[4-7] and several more that mimicked the reduced forms of these active sites.[8-12] These model complexes generally do not reproduce the functions of the biological systems, perhaps in part because many of them are coordinatively saturated or have ligand systems with a different set of donor atoms than is present in the enzyme active site. For example, until recently[11] there were no model compounds with one nitrogen donor per iron, as is found in the active sites of the MMO hydroxylase and the R2 protein of ribonucleotide

reductase. Developing functional models of these enzymes may require even closer approximations of the structures in the proteins. An example of one such effort in modeling hemerythrin is described in Chapter 2.

Another aspect of proteins that can be imitated in the development of functional models is the effect of the protein framework which surrounds the active site. The folded protein chain not only stabilizes the structure of the diiron core, but its bulk also prevents decomposition by reaction with another dimetallic center. In modeling heme proteins like hemoglobin and cytochromes P-450, chemists have built sterically bulky "picket fence" and "strapped" porphyrins successfully to reproduce this effect of the protein framework.[13] Other efforts have focused on encapsulating iron porphyrins and iron phthalocyanines inside a zeolite in order to block bimolecular decomposition of the catalyst.[14] The work described in Chapter 3 seeks to extend this zeolite strategy to the chemistry of non-heme iron model complexes.

Metalloproteins determine what reactions take place at the metal center through a combination of the ligands they provide, structural constraints on the geometry around the metal atoms, and the chemical environment provided by the surrounding protein framework. In modeling dinuclear non-heme iron proteins, the goal is to mimic certain aspects of the active site in order to elucidate which factors are most important. Whether by using a very similar ligand environment or by encapsulating a complex in a zeolite to model the effect of the protein framework, these efforts may ultimately lead to the preparation of functional models for the proteins, which have potential as useful catalysts.

References

(1)   Stenkamp, R. E. *Chem. Rev.* **1994**, *94*, 715-726 and references cited therein.

(2)   Liu, K. E.; Lippard, S. J. In *Advances in Inorganic Chemistry*; Sykes, A. G., Eds.; Academic Press, Inc.: San Diego, 1995; Vol. 42; pp 263-289 and references cited therein.

(3)   Fontecave, M.; Nordlund, P.; Eklund, H.; Reichard, P. In *Advances in Enzymology and Related Areas of Molecular Biology*; Meister, A., Eds.; John Wiley and Sons: New York, 1992; Vol. 65; pp 147-183 and references cited therein.

(4)   Armstrong, W. H.; Lippard, S. J. *J. Am. Chem. Soc.* **1983**, *105*, 4837-4838.

(5)   Wieghardt, K.; Pohl, K.; Gebert, W. *Angew. Chem. Int. Ed. Engl.* **1983**, *22*, 727.

(6)   Mauerer, B.; Crane, J.; Schuler, J.; Wieghardt, K.; Nuber, B. *Angew. Chem. Int. Ed. Engl.* **1993**, *32*, 289-291.

(7)   Que, L., Jr.; True, A. E. In *Progress in Inorganic Chemistry*; Lippard, S. J., Eds.; John Wiley and Sons: New York, 1990; Vol. 38; pp 97-200.

(8)   Chaudhuri, P.; Wieghardt, K.; Nuber, B.; Weiss, J. *Angew. Chem. Int. Ed. Engl.* **1985**, *24*, 778-779.

(9)   Tolman, W. B.; Liu, S.; Bentsen, J. G.; Lippard, S. J. *J. Am. Chem. Soc.* **1991**, *113*, 152-164.

(10)   Dong, Y.; Menage, S.; Brennan, B. A.; Elgren, T. E.; Jang, H. G.; Pearce, L. L.; Que, L., Jr. *J. Am. Chem. Soc.* **1993**, *115*, 1851-1859.

(11)   Herold, S.; Pence, L. E.; Lippard, S. J. *J. Am. Chem. Soc.* **1995**, *117*, 6134-6135.

(12)   Coucouvanis, D.; Reynolds, R. A., III; Dunham, W. R. *J. Am. Chem. Soc.* **1995**, *117*, 7570-7571.

(13)   Collman, J. P.; Halpern, T. R.; Suslick, K. S. In *Metal-Ion Activation of Dioxygen*; Spiro, T. G., Eds.; Wilely-Interscience: New York, 1980; pp 1-72.

(14)   Bedioui, F. *Coord. Chem. Rev.* **1995**, *44*, 39-68.

Chapter 2

Studies in Biomimetic Diiron(III) Chemistry

Introduction

Dinuclear iron centers bridged by carboxylates appear at the active sites of several non-heme iron proteins, including hemerythrin (Hr),[1] the R2 subunit of ribonucleotide reductase (RNR),[2] and soluble methane monooxygenase (sMMO).[3] The diiron(II) forms of all three of these proteins react with dioxygen, but the proteins perform very different functions. Whereas sMMO and RNR react irreversibly with O_2 in the hydroxylation of methane and the generation of a tyrosyl radical, respectively, Hr binds dioxygen reversibly.[4] Hemerythrin also differs from the other two proteins in that it has predominantly histidines in the coordination sphere of the diiron moiety,[1] whereas sMMO and RNR each have only such ligands.[2,3] These differences in coordination environment are a major factor in the unique reactivity of hemerythrin, but may not be sufficient to account for the reversibility of dioxygen binding. Preparation and characterization of a functional model with the same donor set found in the active site of Hr could help identify other characteristics of the protein that are necessary for reversible oxygen binding.

Background. Hemerythrin is the dioxygen carrier in the blood of various marine invertebrates. Extensive structural work has been done on Hr, so that the crystal structures of the oxy-, deoxy-, met- and azidomet- forms of the protein have all been solved.[1,5-8] Much is known about the dioxygen carrier as a result of these studies and others.[9] In deoxyhemerythrin, the two iron(II) ions are bridged by two protein-derived carboxylates and a solvent-derived hydroxide, and five histidines are also bound to the iron atoms. A key feature of this protein complex is that the core is asymmetric (Figure 2.1). One iron is six-coordinate, with three of the histidines bound, whereas the other iron is only five-coordinate.[1] The open coordination site on the latter metal ion is where

dioxygen and other exogenous ligands bind. It is therefore vital to the activity of the protein.

Deoxyhemerythrin   **Oxyhemerythrin**
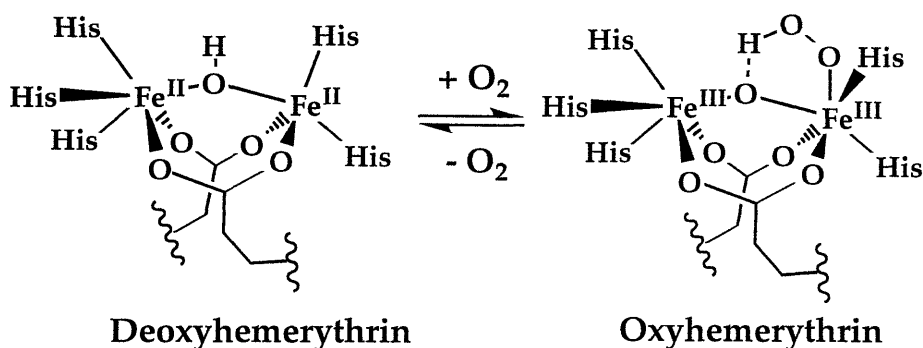
Figure 2.1: Reversible Dioxygen Binding in Hemerythrin

Binding of dioxygen is accompanied by two-electron transfer, oxidizing the iron atoms to the ferric oxidation state and reducing dioxygen to peroxide.[4,9] In addition, there is substantial evidence that a proton is almost simultaneously transferred from the hydroxide bridge to the resulting peroxide, producing the hydroperoxide ligand seen in oxyhemerythrin, as shown in Figure 2.1.[9,10] The stability of the complex is increased by the presence of a hydrogen bond between the hydroperoxide ligand and the oxo bridge. Protonation of the peroxide may also enhance the reversibility of the reaction by reducing π-interactions between the peroxide and the metal.[4]

Early models for the diiron center in Hr were successful in reproducing the (μ-oxo)bis(μ-carboxylato)diiron(III) core in azidomethemerythrin, as well as the spectroscopic and magnetic characteristics of the protein.[11,12] Another complex mimicked the structure, spectroscopy, and magnetic properties of the diiron(II) core in deoxyhemerythrin, including a bridging hydroxide.[13] All of these compounds, however, relied on facially-capping tridentate nitrogen donors to stabilize the complex and prevent formation of higher nuclearity compounds. As a result, none of them had an open coordination site to bind dioxygen or other nucleophiles, as in deoxy-Hr. Other models have used a mixture of

14

bidentate and monodentate capping ligands on each iron(III),[14] but formation of higher nuclearity species has often been a problem in extending this chemistry to diferrous complexes.[15] More recently, an asymmetric diiron(III) model has been synthesized with a tridentate capping ligand on one iron and a bidentate nitrogen donor on the other, with water bound at the remaining site.[16] Interestingly, this complex catalyzes the disproportionation of hydrogen peroxide, rather than binding hydroperoxide to form a stable oxyhemerythrin model.

H₂XDK   Compound 5
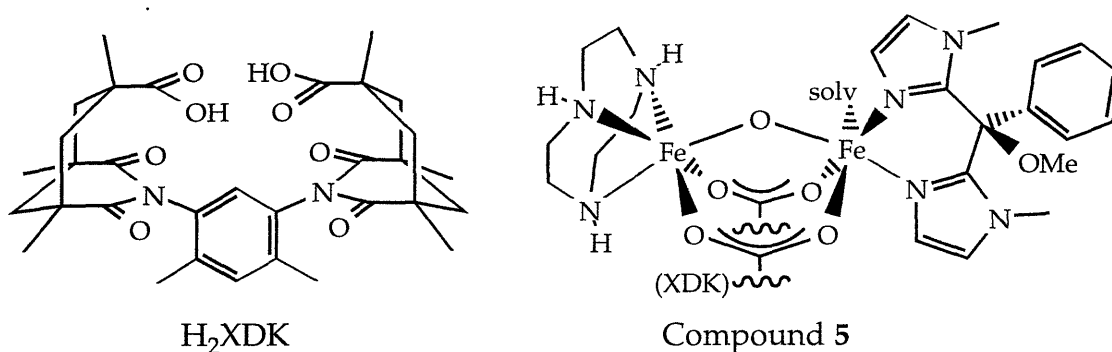
Figure 2.2: A New Model for Methemerythrin

In the work described here, a similarly asymmetric model for hemerythrin has been synthesized, with the primary difference being the use of the dinucleating dicarboxylate ligand xylylenediamine-bis(Kemp's triacid)imide (XDK). This ligand allows direct assembly of a (μ-oxo)bis(μ-carboxylato)diiron(III) unit without any need for anionic or multidentate capping ligands to prevent formation of higher nuclearity species.[17] The resulting solvento diiron(III) complex has proved to be an excellent precursor for the preparation of the asymmetric compound shown in Figure 2.2. This new model for methemerythrin shares with the asymmetric diiron(III) model prepared by Wieghardt, et. al.[16] the ability to catalyze the disproportionation of hydrogen peroxide. In addition, it can form a 1:1 complex with azide which is remarkably

similar to azidomethemerythrin in its spectroscopic characteristics. Compound **5** is an accurate structural model for hemerythrin, but it may not be a functional model even in its reduced form.

Experimental[a]

General. Most solvents were used as received or dried over molecular sieves. The following compounds were synthesized according to literature procedures: BIPhMe,[15] Me$_3$tacn,[18] H$_2$XDK,[19] and [Fe$_2$O(XDK)(MeOH)$_5$-(H$_2$O)](NO$_3$)$_2$·4H$_2$O.[17] Also, tacn·3H$_2$SO$_4$ was made and isolated through a combination of published procedures,[18,20] and neutral tacn was isolated by allowing tacn·3H$_2$SO$_4$ to react with 3 equiv of Ba(OH)$_2$ in water, filtering off BaSO$_4$, and evaporating the water. Nonaqueous hydrogen peroxide was prepared as described in Chapter 3.

The UV/visible spectra were collected on either a Cary 1E Spectrophotometer or on a Hewlett Packard Diode Array Spectrophotometer.

Preparation of [Fe$_2$O(XDK)(BIPhMe)$_2$(H$_2$O)$_2$](NO$_3$)$_2$, 1. To a suspension of 30 mg (0.052 mmol) of H$_2$XDK and 14.6 mg (0.052 mmol) of BIPhMe in 1 mL of methanol was added 14.3 μL (0.10 mmol) of triethylamine. After stirring for 5 min and filtering, 21 mg (0.052 mmol) of Fe(NO$_3$)$_3$·9H$_2$O was added as solid, producing a clear brown solution. Vapor diffusion of ether into the reaction mixture gave 34 mg of brown solid. This powder was recrystallized from a 2:1 mixture of CH$_2$Cl$_2$/MeOH by Et$_2$O vapor diffusion to yield 23 mg (61% yield based on iron) of brown solid. FT-IR (KBr, cm^{-1}): 3130 (m, b); 2965, 2930 (m); 1734 (m); 1695 (s); 1548 (m); 1499 (m); 1470, 1451 (m); 1400 (m); 1361 (m); 1285 (s); 1195

---

[a] Abbreviations: BIPhMe: bis(1-methyl-2-imidazolyl)phenylmethoxymethane
                    tacn: 1, 4, 7-triazacyclononane
                    Me$_3$tacn: 1, 4, 7-trimethyl-1, 4, 7-triazacyclonane
                    H$_2$XDK: m-xylylenediamine bis(Kemp's triacid imide)

(s); 1088, 1072 (w); 986 (m); 959 (w); 899 (m); 762 (s); 721, 703 (m). UV/vis (CH$_3$OH), λ_{max}, nm (ε, M^{-1} cm^{-1}): 342 (5030), 372 (4700), 490 (820), 718 (112). This compound was also prepared by addition of 52 mg (0.185 mmol) of BIPhMe in 1 mL of DMF to 100 mg (0.093 mmol) of [Fe$_2$O(XDK)(MeOH)$_5$(H$_2$O)](NO$_3$)$_2$ in 2.0 mL of DMF. The solution was stirred for 1 h as the color changed from green to brown. Addition of 1 volume of benzene and vapor diffusion of Et$_2$O yielded 116 mg (80%) of **1**. Anal. Calcd for **1**·DMF·H$_2$O, C$_{67}$H$_{87}$N$_{13}$O$_{21}$Fe$_2$: C, 52.87; H, 5.76; N, 11.96. Found: C, 53.07; H, 5.79; N, 12.20. DMF is evident in the IR spectrum of the vacuum-dried material as an additional carbonyl stretch at 1648 cm^{-1}.

Preparation of [Fe$_2$O(XDK)(tacn)$_2$](BF$_4$)$_2$, 2. To a suspension of 28 mg (0.048 mmol) of H$_2$XDK in 1.5 mL of methanol was added 13.5 µL (0.10 mmol) of triethylamine. A suspension of 20 mg (0.069 mmol) of Fe(tacn)Cl$_3$ in 1 mL of MeOH was then added. To this suspension was added 58 mg (0.20 mmol) of solid Tl(BF$_4$), yielding an orange solution with a mostly colorless precipitate, which was removed by filtration. Red-orange crystals of the product were obtained by mixing the orange solution with 1 volume of CH$_2$Cl$_2$ and crystallizing by Et$_2$O vapor diffusion. X-ray diffraction data were collected on one of these crystals, and a crude crystal structure was obtained which revealed the expected connectivity as well as the presence of a thallium atom in the lattice. Due to the poor quality of the data, however, refinement of this structure was not attempted. FT-IR (KBr, cm^{-1}): 3310 (m, N-H); 3150 (m, b); 2978, 2933 (m); 2882 (w); 1730 (m); 1690 (s); 1533 (m); 1465 (m); 1403, 1364 (m); 1229 (w); 1199 (m); 1060 (vs); 928 (m); 764 (m); 743 (w). UV/vis (CH$_2$Cl$_2$), λ_{max}, nm (ε, M^{-1} cm^{-1}): 336 (5430), 478 (986), 510 (sh), 740 (130).

Preparation of [Fe$_2$O(XDK)(DMSO)$_6$](NO$_3$)$_2$·DMSO, 3·DMSO. A solution of 200 mg of [Fe$_2$O(XDK)(MeOH)$_5$(H$_2$O)](NO$_3$)$_2$ in 4.0 mL of DMSO was prepared and filtered. Addition of 3-4 volumes of acetone and crystallization in an Et$_2$O

vapor diffusion chamber yielded 190 mg (75%) of purplish plate-like crystals, some of which were X-ray quality. Anal. Calcd. for $C_{46}H_{80}N_4O_{22}S_7Fe_2$: C, 40.12; H, 5.85; N, 4.07; S, 16.30. Found: C, 40.17; H, 5.88; N, 4.05; S, 15.40. Although the %S is not within error, it can be explained by the partial evaporation of the lattice DMSO molecule during vacuum drying. FT-IR (KBr, cm^{-1}): 3130 (br); 2967, 2928 (m); 1732 (m); 1692 (s); 1546, 1508, 1463 (m); 1384, 1360 (s); 1282 (m); 1193 (s); 991, 958 (s); 763, 743 (m); 442 (s). UV/vis (DMSO), λ_{max}, nm (ε, M^{-1} cm^{-1}): 362 (4770), 476 (382), 590 (146).

Preparation of [Fe$_2$(OH)(XDK)(BIPhMe)(H$_2$O)(NO$_3$)$_3$]·CH$_3$OH·5H$_2$O, 4·CH$_3$OH·5H$_2$O. To a suspension of 30 mg (0.052 mmol) of H$_2$XDK in 1.5 mL of MeOH was added 42 mg (0.104 mmol) of Fe(NO$_3$)$_3$·9H$_2$O, generating [Fe$_2$O(XDK)(MeOH)$_5$(H$_2$O)](NO$_3$)$_2$ in situ. A solution of 14 mg (0.050 mmol) of BIPhMe in 0.75 mL of MeOH was added dropwise over 20 min to the green solution, with no significant color change. An equal volume of CH$_2$Cl$_2$ was added, and yellow crystals were obtained by Et$_2$O vapor diffusion. Yield 44 mg (70%). Anal. Calcd. for $C_{49}H_{73}N_9O_{26}Fe_2$: C, 44.73; H, 5.59; N, 9.58. Found: C, 44.57; H, 5.61; N, 9.47. FT-IR (KBr, cm^{-1}): 3140 (m); 2965, 2930 (m); 1736 (m); 1696 (s); 1538 (s); 1500 (s); 1462 (m); 1406, 1383, 1359 (m); 1282 (s); 1186 (s); 990 (m); 958 (m); 762 (s); 723, 703 (m); 439 (m). See below for a discussion of the UV/visible spectrum.

Preparation of [Fe$_2$O(XDK)(tacn)(BIPhMe)(H$_2$O)](NO$_3$)$_2$, 5(NO$_3$)$_2$. To a solution of 625 mg (0.58 mmol) of [Fe$_2$O(XDK)(MeOH)$_5$(H$_2$O)](NO$_3$)$_2$·4H$_2$O in 7.0 mL of DMF was added, dropwise over 10 min, a solution of 164 mg (0.58 mmol) of BIPhMe in 1.0 mL of MeOH. After stirring for one hour, 75 mg of tacn in 1.5 mL of EtOH was added dropwise, changing the green solution to brown. The product was precipitated from the reaction mixture by vapor diffusion of ether or by mixing the solution with benzene or toluene, followed by vapor diffusion of

18

Et$_2$O or t-BuOMe, yielding 550 mg (69%) total. FT-IR (KBr, cm^{-1}): 3304 (w); 2965 (m); 2930 (m); 1731 (m); 1691 (s); 1648 (m); 1543 (m); 1499 (m); 1464 (m); 1382 (s); 1362 (s); 1284 (m); 1195 (m); 1092, 988, 959 (w); 764 (m); 723, 703 (w); 428 (m). UV/vis (DMF), λ_{max}, nm (ε, M^{-1} cm^{-1}): 336 (6700), 366 (sh), 471 (1040), 498 (990), 743 (143) [726 (130) in CHCl$_3$; 700 (148) in DMSO]. Anal. Calcd. for 5(NO$_3$)$_2$·DMF·2H$_2$O, C$_{57}$H$_{84}$N$_{12}$O$_{20}$Fe$_2$: C, 50.00; H, 6.18; N, 12.28. Found: C, 49.76; H, 6.15; N, 12.29.

Complex **5** was also prepared with different counterions X = ClO$_4$$^-$, PF$_6$$^-$, and BF$_4$$^-$ by addition of 4 equiv of Bu$_4$NX to the reaction mixture before crystallization. Crystals of the perchlorate salt were studied by X-ray diffraction, but due to the poor quality of these crystals, the structure could not be solved. The unit cell parameters obtained in the attempted structure solution are given in Table 2.9. These crystals were also sent for analysis, and the results for C, H, and N, as well as the size of the unit cell, are consistent with the composition 5(ClO$_4$)$_2$·4DMF. Anal. Calcd. for C$_{66}$H$_{101}$N$_{13}$O$_{23}$Cl$_2$Fe$_2$: C, 48.72; H, 6.26; N, 11.19; Cl, 4.35. Found: C, 48.55; H, 5.95; N, 11.28; Cl, 1.59. The %Cl is low despite the presence of a strong perchlorate stretch in the IR spectrum. Partially replacing ClO$_4$$^-$ with NO$_3$$^-$ leads to inconsistent results for C, H, and N.

Preparation of 5(BPh$_4$)$_2$ was attempted by precipitation of the complex from a methanol solution of 5(NO$_3$)$_2$ with NaBPh$_4$, followed by recrystallization from acetonitrile by ether vapor diffusion. Unfortunately, the precipitated complex did not contain BIPhMe, as indicated by the absence of the IR stretch at 1284 cm^{-1}. The BIPhMe ligand was also recovered in 100% yield from the methanol supernatant.

Preparation of [Fe$_2$O(XDK)(tacn)(BIPhMe)(N$_3$)](NO$_3$), 6(NO$_3$). To a solution of 75 mg (5.5 x 10^{-5} mol) of 5(NO$_3$)$_2$ in 2.5 mL of acetonitrile was added 0.2 mL of a 0.28 M solution of NaN$_3$ (5.5 x 10^{-5} mol total) in MeOH, resulting in a

darkening of the solution. After crystallization by Et_2O vapor diffusion, a mixture of dark solids and pale, powdery clusters was collected. FT-IR of dark solids (KBr, cm^{-1}): 3304 (w); 2965 (m); 2931 (m); 2049 (s; N_3^- stretch); 1731 (m); 1690 (s); 1558 (m); 1498 (m); 1460 (m); 1398 (s); 1384 (s); 1361 (s); 1284 (w); 1198 (m); 1089, 987, 959 (w); 764 (m); 723, 703 (w); 426 (w). UV/vis (DMF), λ_{max}, nm (ε, M^{-1} cm^{-1}): 330 (6700), 431 (sh, ~3200), 691 (150).

Reaction of 5(BF_4)$_2$ with Hydrogen Peroxide. To a solution of 25 mg of **5** (BF_4)$_2$ in 0.5 mL of DMSO mixed with 1.0 mL of DMF was added 10 drops of 30% aqueous H_2O_2. The brown solution soon became paler, and bubbles began to form after a few seconds. Less bleaching of the solution was observed in a parallel experiment where DMSO was the only solvent. Gas evolution continued for nearly an hour, but addition of more H_2O_2 did not result in resumed bubbling. Two weeks later, colorless crystals had grown in this solution, which turned out to be $H_2XDK \cdot 2DMSO$, as indicated by crystallographic chemical analysis (CCA).

In another experiment, addition of a 90-fold excess of nonaqueous H_2O_2 to 15 mg of **5** (NO_3)$_2$ in 1.0 mL of DMF/DMSO did not result in any color change or gas evolution over the course of 15 min. Subsequent addition of 1 drop of NEt_3 resulted immediately in a rapid gas evolution and a darkening of the solution. Later attempts to reproduce this result with 1 equiv each of H_2O_2 and NEt_3 in dilute solution were not successful. Only the addition of aqueous H_2O_2 led to evolution of gas, accompanied by a bleaching of the visible bands characteristic of oxo-bridged diiron(III) complexes.

X-ray Crystallography

General Procedures. The data for all of the structures were collected on an Enraf-Nonius CAD4 kappa geometry diffractometer using Mo $K\alpha$ radiation. Data collection and reduction, including corrections for Lorentz and polarization

effects, were performed by using general procedures previously described.[21] No appreciable decay was observed for any of the samples, as judged by periodic monitoring of three standard reflections. Initial iron positions were obtained by using the direct methods program SIR-92x for **2**, **3**, and **4**. The remaining heavy atoms were located with DIRDIF phase refinements and difference Fourier maps.[22] The TEXSAN program package was used to refine the structures.[23] A summary of data collection parameters for complexes **3** and **4** is given in Table 2.3, and the parameters used in obtaining the crude structure solution of **2** are listed in Table 2.8.

[Fe$_2$O(XDK)(DMSO)$_6$](NO$_3$)$_2$·DMSO, 3·DMSO. A plate-like dichroic green/purple crystal was mounted on a glass fiber under Paratone N oil. Data collection and structure solution were carried out as described above. No absorption correction was applied. All non-hydrogen atoms were refined anisotropically except for those of a disordered lattice DMSO molecule, which were refined by using isotropic temperature factors. An attempt to fit the electron density of the disordered DMSO resulted in a model in which two positions for the sulfur atom (S402, S403) and three positions (C403, C404, C409) for the two methyl groups were assigned. Hydrogen atoms were included in the final cycles of least-squares refinement at calculated positions. Hydrogen atoms were not included for the disordered methyl groups. The largest electron density peak in the final difference Fourier map was 0.9 e$^-$/Å^3, located near a methyl group (C9) of a bound DMSO molecule. Selected bond distances and angles for **3** are listed in Table 2.4, and the final positional and thermal parameters are given in Table 2.6.

[Fe$_2$(OH)(XDK)(BIPhMe)(H$_2$O)(NO$_3$)$_3$]·CH$_3$OH·5H$_2$O, 4·CH$_3$OH·5H$_2$O. A pale yellow block, obtained by crystallization directly from the reaction mixture, was mounted on the end of a glass fiber under Paratone N oil. Data collection

and structure solution were carried out as described above. No absorption correction was applied. The positions of most non-hydrogen atoms in the molecule were refined with anisotropic thermal parameters. The xylyl ring of XDK was treated as a rigid body. Certain atoms of the two nitrates bound to Fe2, including N9, O7, O8, O18, O20, O21, and O22, were refined with isotropic thermal parameters. The disorder observed for atoms O7 and O21 in these nitrates was modeled by isotropic refinement over two positions at half occupancy each for each nitrate (O7 and O8, O21 and O22). Atomic positions of all the lattice solvents were refined with isotropic thermal parameters, those of the dichloromethane molecule being refined at half occupancy. The hydrogen atoms were included in calculated positions during the final cycles of least-squares refinement. The largest electron density peak in the final difference Fourier map was 1.2 e$^-$/Å^3, located in the lattice near a water molecule. Selected bond distances and angles for **4** are listed in Table 2.5, and the final positional and thermal parameters are given in Table 2.7.

Results and Discussion

Synthesis of Diiron(III) Complexes with XDK. Early attempts to synthesize an asymmetric diiron(III) complex were made by using a procedure in which two different sources of iron were added sequentially to deprotonated XDK, as shown in Method A in Figure 2.3. In theory, the first equivalent of iron could lead to a mononuclear intermediate, which might then react with the second iron compound to give an asymmetric, dinuclear final product.

Figure 2.3: Methods for Preparation of (XDK)diiron(III) Complexes

Method A: H$_2$XDK + 2NEt$_3$ + Fe(tacn)Cl$_3$ + Fe(NO$_3$)$_3$·9H$_2$O + BIPhMe $\xrightarrow{\text{MeOH/CH}_2\text{Cl}_2}$ **1** or **2**

Method B. [Fe$_2$O(XDK)(MeOH)$_5$(H$_2$O)](NO$_3$)$_2$ + BIPhMe + tacn $\xrightarrow{\text{DMF}}$ **5 (NO$_3$)$_2$**
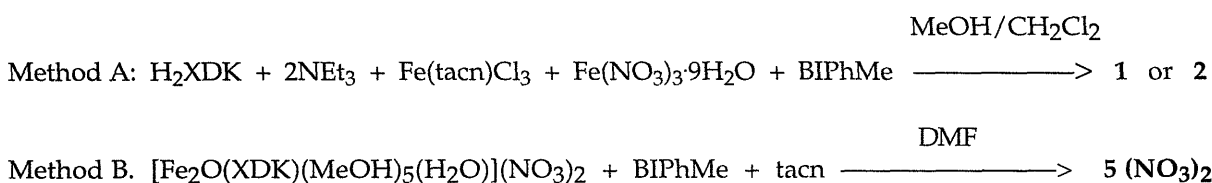
The isolation of compounds 1 and 2, however, demonstrates that addition of a single equivalent of iron(III) to XDK, as in the preparation of 1, rapidly affords a dinuclear oxo-bridged species, as indicated by the UV/visible spectrum of the reaction mixture. Evidently, the self-assembly of an oxo-bridged diiron(III) complex thermodynamically drives formation of dinuclear compounds. The bis(BIPhMe) and bis(tacn) complexes (1 and 2) were also synthesized by direct addition of 2 equiv of ligand to the XDK solvento complex, $[Fe_2O(XDK)(MeOH)_5(H_2O)](NO_3)_2$. These two symmetric complexes proved useful for comparison with the asymmetric hybrid of the two, complex 5, as described below.

At the start of these investigations, the more sterically demanding Me_3tacn was used in place of tacn, primarily because it is incapable of forming FeL_2^{n+} complexes. When $[Fe(Me_3tacn)Cl_3]$ was allowed to react with XDK, or when Me_3tacn was added directly to the XDK solvento complex, however, either no oxo-bridged species could be detected at all by UV/vis spectrophotometry or only starting material was recovered. The reason for these problems became clear when the target complex was modeled on computer by using the CAChE software. When Me_3tacn binds to one iron of a diiron(III)-XDK core, two of the methyl groups on the ligand lie within 2.5 Å of methyl groups on XDK (Figure 2.4). This steric interaction almost certainly prevented formation of a compound containing both XDK and Me_3tacn.

An Asymmetric Diiron(III) Compound. Compound 5, which is designed to have a coordination environment almost identical to that in methemerythrin, is prepared in good yield by reacting a solvento complex first with BIPhMe and then with tacn. The IR spectrum of the resulting material revealed the presence of both of these ligands and XDK. This synthesis was carried out in a variety of solvents, including methanol, DMSO, and DMF. It was

23

thought that strong coordination by solvent molecules such as DMSO would slow formation of a bis(BIPhMe) complex prior to addition of tacn. Crystallizations in DMSO often produced a green, crystalline side product, however. No problems were observed with DMF, and fairly crystalline material was often obtained from this medium. Such polar solvents appear to be necessary to dissolve some of the salts of complex **5**, especially the perchlorate, whereas the nitrate salt is soluble in a somewhat broader range of solvents.

It has proved difficult to get X-ray quality crystals for purposes of determining the precise structure of this putative asymmetric complex. Data were collected on a few weak crystals of $5(ClO_4)_2$, but the structure could not be solved. Unit cell parameters are listed in Table 2.6. The large volume, over 17200 Å^3, is consistent with eight molecules per unit cell, along with at least four DMF molecules per complex. Based on current data, the space group appears to be P222 (#16), although this assignment could change with better quality data. In this space group, there would have to be two molecules in the asymmetric unit, which, given the chiral nature of the supposed structure, may be an indication that the crystal is a racemic mixture of the two stereoisomers.

A sample of $5(NO_3)_2$, prepared by a colleague[24] and crystallized from methanol, was submitted to analysis by MALDI mass spectrometry. Among the many peaks in the mass spectrum was a broad peak with $m/z = 1272$, corresponding to the molecular ion with methanol in the exchangeable site and the nitrates ion-paired with the complex. Molecular ions were also observed for XDK, BIPhMe, and tacn. More significantly, there were no peaks where the molecular ions of **1** and **2** were expected. These data are consistent with the proposed structure of **5**, and indicate that the symmetric complexes are not major contaminants.

Electronic Spectra. The spectroscopic properties of the oxo-bridged diiron(III) core are sensitive to the ligand environment and provide some support for the formulation of complex **5** as an asymmetric (μ-oxo)(XDK)-diiron(III) species containing BIPhMe and tacn. In particular, the lowest-energy band in the UV/vis spectrum, assigned to the $^6A_1 \rightarrow [^4T_2](^4G)$ ligand field transition, shifts to higher wavelength with increasing numbers of nitrogen donor atoms.[17] As shown in Table 2.1, the position of this band in the spectrum of complex **5** falls between the corresponding bands in the spectra of the bis(BIPhMe) and bis(tacn) complexes (**1** and **2**), in agreement with the intermediate number of nitrogen ligands in the asymmetric complex. The intensity of the absorbance at 366 nm in **5** is also intermediate in strength relative to the other two complexes. Except for the peak at 496 nm, however, there is little to distinguish the spectrum of **5** from that of a 50:50 mixture of **1** and **2**, owing to the breadth of the bands (Figure 2.9). The spectra in Table 2.1 and Figure 2.9 were collected in DMSO because the relatively weak ligand field contribution of the coordinated solvent molecule creates more of a difference in the position of the low energy band. In other solvents, the position of this band in the spectra of **1** and **5** shifts to longer wavelength, indicating the presence of at least one exchangeable site where another solvent can bind.

Table 2.1: UV/vis Spectra of (μ-Oxo)(XDK)diiron(III) Complexes in DMSO

Compound	λ_{max} (nm)				
$[Fe_2O(XDK)(BIPhMe)(DMSO)_4](NO_3)_2$		364	474		632
$[Fe_2O(XDK)(BIPhMe)_2(DMSO)_2](NO_3)_2$, **1**	338	372	480		684
$[Fe_2O(XDK)(BIPhMe)(tacn)(DMSO)](NO_3)_2$, **5**	336	366(sh)	472	496	700
$[Fe_2O(XDK)(tacn)_2](BF_4)_2$, **2**	336		478	510(sh)	740

A Model for Azidomethemerythrin. Addition of azide ion to the metHr model complex **5** leads to a significant visible change and formation of compound

6, which presumably has azide bound in the one exchangeable site. Although the crystal structure of this complex could not be obtained, spectroscopic characterization of this product supports this formulation. In a titration of complex **5** with sodium azide in DMF, an isosbestic point is observed at 729 nm, the band at 743 nm being replaced by one at 691 nm arising from **6** (Figure 2.6). This point is constant up through 0.9-1.0 equivalents of azide, beyond which all absorbances above 625 nm decrease. Such behavior is consistent with formation of a 1:1 complex with azide replacing the coordinated solvent molecule, followed by decomposition of the complex, probably because additional azide must displace other ligands, such as the carboxylates of XDK, in order to react.

Table 2.2: UV/vis Spectra of (μ-Oxo)diiron(III) Azide Complexes

Compound	λ_{max} (nm)		
Azidomethemerythrin, HrN_3 [25]	328	445	680
$[Fe_2O(XDK)(BIPhMe)(tacn)(N_3)](NO_3)$, **6**	330	430 (sh)	691

The spectroscopic properties of the azide adduct **6** correspond remarkably well with those of azidomethemerythrin (azidometHr). In the IR spectrum, the azide stretch of 2049 cm^{-1} for compound **6** is virtually identical to that observed in azidomethemerythrin (2050 cm^{-1}).[26] The UV/visible spectra of complex **6** and HrN_3 correlate very well, too, as shown in Table 2.2. Difference spectra obtained in the titration experiment cleanly reveal the growth of an absorption band at 430 nm, which is probably an azide-to-iron charge transfer transition. Previously known model compounds with only tridentate nitrogen-donor capping ligands have imitated the general features of azidometHr before,[12,27] but compound **6** is the first to produce the same spectroscopic signature with a complex containing azide.

Reactions with Hydrogen Peroxide. Addition of 10 drops of 30% aqueous hydrogen peroxide to a solution of compound $5(NO_3)_2$ in DMF/DMSO led to gas evolution and a bleaching of the solution. Bubbles continued to form gradually for almost an hour in this case. In contrast, addition of non-aqueous H_2O_2 did not produce any change in the UV/visible spectrum of the complex. Subsequent addition of a drop of triethylamine in one experiment led immediately to rapid evolution of gas and a darkening of the solution. The latter result was not reproducible in a more dilute solution, however, so the UV/visible spectrum of the darker solution was not obtained. It was observed, on the other hand, that the presence of triethylamine in a dilute solution of the complex promoted very rapid gas evolution with each drop of aqueous H_2O_2 added, such that no more bubbles were observed after a few seconds. Addition of triethylamine and aqueous hydrogen peroxide to a solution containing the symmetric complex **1** resulted in immediate gas evolution and a color change to reddish brown, whereas **1** was completely unreactive to aqueous H_2O_2 alone.

The gas evolution observed in these experiments is most likely due to catalytic disproportionation of hydrogen peroxide into dioxygen and water. Dioxygen production was not quantitatively measured, but the amount of gas evolved was qualitatively much more than a stoichiometric quantity (~0.5 mL of gas at 25°C, 1 atm). Some water appears to be necessary, at least in most cases, but also results in the decomposition of the complex. The presence of base clearly promotes the reaction, perhaps by deprotonating H_2O_2, thereby allowing faster reaction with the metal complex.

This disproportionation reaction is not catalyzed to any significant extent by the symmetric bis(tacn) compound **2**, so it seems that an open or labile coordination site is necessary. In addition, the reactivity of the symmetric bis(BIPhMe) complex **1** differs from that of the asymmetric compound **5** in that it

requires base for a reaction to occur at all. This difference may indicate that different mechanisms are at work in the reactions catalyzed by complexes **1** and **5**. In the latter case, the reaction may proceed through a diiron(III) complex with hydroperoxide bound in the open site, which decomposes to O_2 in analogy to dioxygen release from the protein (Figure 2.5). Such an intermediate has been proposed for the catalase-like activity exhibited by a very similar compound prepared by Wieghardt, et. al., which has the same asymmetric coordination environment with one open site.[16] In contrast, the mechanism involved in the activity of complex **1** may require that H_2O_2 be deprotonated twice in order to bind as a 1,2-μ-peroxo or to interact with another metal complex.

Significantly, catalase activity has not been observed for methemerythrin itself, despite attempts to react it with hydrogen peroxide,[25] although the reduced form, deoxyHr, reacts with H_2O_2 to give hydroxymetHr.[28] The inability to obtain the bound hydroperoxide of oxyhemerythrin with H_2O_2 was attributed to the fact that the protein is not stable at the high pH where significant amounts of HO_2^- are present in aqueous H_2O_2. This fact most likely does not explain the lack of catalase activity in hemerythrin, however, since Wieghardt's asymmetric model catalyzes the disproportionation reaction in aqueous solution at pH 4-6.[16] The main difference between oxyHr and the asymmetric model complexes appears to be the stability of the hydroperoxide. In air-saturated buffer, the equilibrium favors the oxyHr form of the protein,[25] whereas release of dioxygen is apparently favored in the model complexes. A more positive redox potential for the model complexes relative to the active site of hemerythrin or a more nucleophilic oxo bridge might shift the equilibrium towards O_2 release. This step could be followed by rapid reduction of H_2O_2 by the diiron(II) form of the complex. The latter process could even be bimolecular, involving a reaction between a diiron(III)-hydroperoxide complex and the reduced dinuclear metal center. Such

28

a mechanism would be blocked by the protein framework of hemerythrin, which might explain why catalase activity is not observed for the protein.

A DMSO Solvento Complex. A new solvento complex, **3**, with six DMSO molecules bound to a (μ-oxo)(XDK)diiron(III) core, can be isolated by dissolving the previously known methanol solvento complex in DMSO, and crystallizing with acetone and ether. Spectroscopically, the different solvent results in a shift of the low energy band in the visible spectrum from 614 nm in methanol to 590 nm in DMSO, consistent with the weaker ligand field contribution of the DMSO ligands. The coordinated solvent molecules are still easily replaced by added ligands such as tacn and BIPhMe, allowing synthesis of compounds such as the oxo-bridged analogue of complex **4** in an aprotic medium.

Compound **3** crystallizes in the triclinic space group P$\bar{1}$. An ORTEP drawing of the structure is shown in Figure 2.7. The complex has the expected core of two essentially octahedral iron atoms bridged by an oxo ligand and the carboxylates of XDK. Six DMSO molecules are bound in the terminal sites through the oxygen atom, with the methyl groups pointing away from the diiron center. The primary deviation from octahedral of the geometry at each iron is that all the O(oxo)-Fe-O(cis) angles are > 90°. The (μ-oxo)(XDK)diiron(III) core of this structure is very similar to the methanol solvento complex, with a slightly wider Fe-O-Fe angle (125°) relative to that of $[Fe_2O(XDK)(MeOH)_5(H_2O)]^{2+}$ (122°).[17] The Fe-O(DMSO) bond lengths are all roughly equivalent, regardless of whether the ligand is cis or trans to the oxo bridge. This characteristic of equivalent bond lengths is shared by several other complexes with only monodentate capping ligands.[17] Selected bond distances and angles for **3** are given in Table 2.4, and final positional and thermal parameters are listed in Table 2.6.

All the DMSO ligands bind to iron through the oxygen lone pair trans to the methyl groups. This coordination mode allows a variety of different orientations for the DMSO molecule relative to the Fe···Fe vector. The distances of the DMSO methyl groups from the nearest iron range from 4.0-4.6 Å. Interestingly, the lower limit of this Fe···C distance supports the conclusion of ENDOR studies of the mixed-valence form of MMOH treated with DMSO, in which a ^{13}C-labeled DMSO is proposed to be O-bound to iron(III) based on the distance-dependent coupling between the unpaired electron and the ^{13}C nucleus.[29]

Solid State Structure of a Hydroxo-Bridged Diiron(III) Complex. An unusual carboxylate-bridged diiron(III)-XDK complex, [Fe$_2$(OH)(XDK)(BIPhMe)-(H$_2$O)(NO$_3$)$_3$] (4), is obtained in crystalline form by allowing the MeOH solvento complex to react with one equivalent of BIPhMe. An ORTEP drawing of the complex is shown in Figure 2.8 and selected bond distances and angles are given in Table 2.5. The two iron atoms in the asymmetric neutral complex are essentially octahedral and bridged by the carboxylates of XDK and a hydroxide ion. BIPhMe and a nitrate occupy the terminal sites on Fe1 and two nitrates and a water molecule are bound terminally to Fe2. The Fe-O(bridging) bond lengths of 1.94 and 1.96 Å and the relatively long Fe···Fe distance of 3.45 Å are typical of hydroxide-bridged diiron(III) complexes.[30] The positive charge on the iron atoms is balanced by XDK, the three nitrates, and the hydroxide. A strong bifurcated hydrogen bond from the bridging hydroxide oxygen atom to two of the nitrate oxygen atoms, O3 (O3···O1, 2.80 Å) and O7 (O7···O1, 2.79 Å), also supports hydroxide as the bridging moiety, although the hydrogen could not be located in the difference Fourier map. The coordinated water molecule, O10, which is trans to the hydroxo bridge, is also involved in hydrogen bonding to a water molecule in the lattice, O19 (O10···O19, 2.6 Å), which is in turn hydrogen-bonded to two

imide oxygens of the XDK ligand. Final positional and thermal parameters for **4** are listed in Table 2.7.

In solution, this mono(BIPhMe)-substituted compound is largely deprotonated, existing as an oxo-bridged diiron(III), as evidenced by the characteristic visible absorption bands at 474 and 632 nm (in DMSO). The intensity of these features is significantly affected by solvent, though, being most intense in solvents with a high dielectric constant, such as DMSO or DMF. When the medium is a mixture of methanol and dichloromethane, as in the crystallization, the absorptivity of the low energy band, which shifts to 670 nm in methanolic solution, is reduced by roughly 25%. Under these conditions, addition of only 0.1 equivalents of methanolic HNO_3 causes the disappearance of both ligand-field transitions. This behavior suggests that in methanolic solution, the oxo-bridged species is in equilibrium with its hydroxo-bridged analogue. In solvent systems with lower dielectric constants, the degree of protonation of the oxo bridge is increased because coordination of the nitrate counterions is favored, increasing the basicity of the oxo bridge by virtue of their charge, and stabilizing the bridging hydroxide by hydrogen bonding.

Conclusion

None of the diiron(III) complexes described here is a functional model for hemerythrin. The chemistry of complex **5**, which has a set of donor atoms for the diiron center that is almost identical to that found in Hr, does help to identify the characteristics of the protein that are important to reversible dioxygen binding. Five nitrogen donors and one open site, in addition to the two bridging carboxylates and oxo or hydroxo bridge, are not sufficient to produce a functional model. If a key intermediate in the catalase activity of the asymmetric model complex is a bound hydroperoxide analogous to the structure of oxyHr, this

31

species is not as stable in the model compound as it is in hemerythrin. In the protein such factors as the redox potential of the metal center or the pK_a of the hydroxo bridge may be tuned by the specific geometry of the active site to stabilize the oxyHr form. Another important factor could be the protein framework which prevents the bound hydroperoxide from reacting with another dinuclear complex. Given the lack of such a framework in the model complex it is possible that the catalase activity proceeds by an unknown mechanism, possibly involving a bimolecular step, having nothing in common with reversible dioxygen binding in hemerythrin. Further study of the kinetics of the disproportionation reaction, and possibly reduction of the diiron(III) center, will help to elucidate these issues.

References

(1)   Stenkamp, R. E.; Sieker, L. C.; Jensen, L. H. *J. Am. Chem. Soc.* **1984**, *106*, 618-622.

(2)   Nordlund, P.; Sjöberg, B.-M.; Eklund, H. *Nature* **1990**, *345*, 593-598.

(3)   Rosenzweig, A. C.; Frederick, C. A.; Lippard, S. J.; Nordlund, P. *Nature* **1993**, *366*, 537-543.

(4)   Feig, A. L.; Lippard, S. J. *Chem. Rev.* **1994**, *94*, 759-806.

(5)   Holmes, M.; Trong, I. L.; Turley, S.; Sieker, L. C.; Stenkamp, R. E. *J. Mol. Biol.* **1991**, *218*, 583-593.

(6)   Sheriff, S.; Hendrickson, W. A.; Smith, J. L. *Life Chem. Rep. Suppl. Ser.* **1983**, *1*, 305.

(7)   Sheriff, S.; Hendrickson, W. A.; L., S. J. *J. Mol. Biol.* **1987**, *197*, 273.

(8)   Holmes, M. A.; Stenkamp, R. E. *J. Mol. Biol.* **1991**, *220*, 723-737.

(9)   Stenkamp, R. E. *Chem. Rev.* **1994**, *94*, 715-726.

(10)   Kramarz, K. W.; Norton, J. R. In *Progress in Inorganic Chemistry*; Karlin, K. D., Eds.; John Wiley & Sons: New York, 1994; Vol. 42; pp 1-66.

(11)   Armstrong, W. H.; Spool, A.; Papaefthymiou, G. C.; Frankel, R. B.; Lippard, S. J. *J. Am. Chem. Soc.* **1984**, *106*, 3653-3667.

(12)   Wieghardt, K.; Pohl, K.; Gebert, W. *Angew. Chem. Int. Ed. Engl.* **1983**, *22*, 727.

(13)   Chaudhuri, P.; Wieghardt, K.; Nuber, B.; Weiss, J. *Angew. Chem. Int. Ed. Engl.* **1985**, *24*, 778-779.

(14)   Taft, K. L.; Masschelein, A.; Liu, S.; Lippard, S. J.; Garfinkel-Shweky, D.; Bino, A. *Inorg. Chim. Acta* **1992**, *198-200*, 627-631.

(15)   Tolman, W. B.; Liu, S.; Bentsen, J. G.; Lippard, S. J. *J. Am. Chem. Soc.* **1991**, *113*, 152-164.

(16)   Mauerer, B.; Crane, J.; Schuler, J.; Wieghardt, K.; Nuber, B. *Angew. Chem. Int. Ed. Engl.* **1993**, *32*, 289-291.

(17)   Watton, S. P.; Masschelein, A.; Rebek, J., Jr.; Lippard, S. J. *J. Am. Chem. Soc.* **1994**, *116*, 5196-5205.

(18)   Madison, S. A.; Batal, D. J. International Patent #WO 94/00439. *World Intellectual Property Organization*; 1994.

(19)   Rebek, J., Jr.; Marshall, L.; Wolak, R.; Parris, K.; Killoran, M.; Askew, B.; Nemeth, D.; Islam, N. *J. Am. Chem. Soc.* **1985**, *107*, 7476-7481.

(20)   Searle, G. H.; Geue, R. J. *Aust. J. Chem.* **1984**, *37*, 959-970.

(21)   Carnahan, E. M.; Rardin, R. L.; Bott, S. G.; Lippard, S. J. *Inorg. Chem.* **1992**, *31*, 5193-5201.

(22)   Parthasarathi, V.; Beurskens, P. T.; Slot, H. J. B. *Acta Crystallogr.* **1983**, *A39*, 860-864.

(23)   TEXSAN: Single Crystal Structure Analysis Software, V. 5.0; Molecular Structure Corporation; The Woodlands, TX, 1989.

(24)   Barrios, A. M.; Lippard, S. J. unpublished results.

(25)   Keresztes-Nagy, S.; Klotz, I. M. *Biochemistry* **1965**, *4*, 919-931.

(26)   Klotz, I. M.; Kurtz, D. M. *Acc. Chem. Res.* **1984**, *17*, 16.

(27)   Armstrong, W. H.; Lippard, S. J. *J. Am. Chem. Soc.* **1983**, *105*, 4837-4838.

(28)   Armstrong, G. D.; Sykes, A. G. *Inorg. Chem.* **1986**, *25*, 3514-3516.

(29)   DeRose, V. J.; Liu, K. E.; Lippard, S. J.; Hoffman, B. M. *J. Am. Chem. Soc.* in press.

(30)   Turowski, P. N.; Armstrong, W. H.; Liu, S.; Brown, S. N.; Lippard, S. J. *Inorg. Chem.* **1994**, *33*, 636-645.

Table 2.3: Crystallographic Information for Complexes **3** and **4**

Compound	3·2DMSO·Me_2CO·H_2O	4·5H_2O·0.5CH_2Cl_2
Formula	$C_{51}H_{94}N_4O_{25}S_8Fe_2$	$C_{48.5}H_{70}N_9O_{25}ClFe_2$
Formula Weight, g/mol	1531.49	1326.3
Crystal Size, mm	0.6 x 0.29 x 0.06	0.38 x 0.30 x 0.23
Crystal System	triclinic	monoclinic
Space Group	P$\bar{1}$	C2/c
a, Å	14.674(1)	25.394(8)
b, Å	16.787(5)	17.400(2)
c, Å	16.858(4)	32.934(9)
α, deg	103.32(2)	
β, deg	97.16(1)	113.95(3)
γ, deg	114.79(2)	
Volume, Å^3	3552(2)	13298(6)
Z	2	8
Density (calc.), g/cm^3	1.43	1.31
Temperature, K	183.5	183.5
Abs. coeff., cm^{-1}	7.19	5.54
Trans. coeff., min/max	0.755 - 1.000	0.948 - 1.000
2θ Range, deg	3 < 2θ < 48	3 < 2θ < 48
Index Range	+h, ±k, ±l	±h, +k, +l
No. of data collected	11824	11234
p-factor[a]	0.030	0.031
R_{av}	0.05	0.02
No. of independent data	11118	10825
No. of obs. unique data[b]	6833	4944
No. of parameters	794	667
Data/parameter ratio	8.6	7.4
R[c]	7.21	10.36
R_w	7.47	12.74
GOF	1.74	2.82
Largest shift/esd, final	0.00	0.25
Largest peak, e$^-$/Å^3	0.9	1.2

[a] Used in the calculation of $\sigma(F^2)$. [b]Observation criterion I > 3σ(I). [c] R = $\Sigma||F_o|-|F_c||/\Sigma|F_o|$, R_w = $[\Sigma w(|F_o|-|F_c|)^2/\Sigma w|F_o|^2]^{1/2}$, where w = 1/$\sigma^2$(F), as defined in ref 21.

Table 2.4: Selected Bond Distances and Angles for [Fe$_2$O(XDK)(DMSO)$_6$](NO$_3$)$_2$, **3**

Bond Distances (Å)

Fe1-O7(oxo)	1.799(5)	Fe2-O7(oxo)	1.795(5) Å
Fe1-O1	2.089(5)	Fe2-O4	2.077(5)
Fe1-O2	2.076(5)	Fe2-O5	2.082(5)
Fe1-O3	2.077(5)	Fe2-O6	2.086(5)
Fe1-O101	2.055(5)	Fe2-O102	2.058(5)
Fe1-O201	2.045(5)	Fe2-O202	2.065(5)

Bond Angles (deg)

Fe1-O7-Fe2	125.2(3)	O4-Fe2-O5	86.3(2)
O1-Fe1-O2	85.3(2)	O4-Fe2-O6	87.4(2)
O1-Fe1-O3	87.3(2)	O4-Fe2-O7	93.7(2)
O1-Fe1-O7	93.8(2)	O4-Fe2-O102	171.6(2)
O1-Fe1-O101	170.5(2)	O4-Fe2-O202	86.8(2)
O1-Fe1-O201	87.2(2)	O5-Fe2-O6	85.0(2)
O2-Fe1-O3	85.0(2)	O5-Fe2-O7	97.3(2)
O2-Fe1-O7	95.2(2)	O5-Fe2-O102	89.1(2)
O2-Fe1-O101	88.4(2)	O5-Fe2-O202	166.5(2)
O2-Fe1-O201	166.7(2)	O6-Fe2-O7	177.5(2)
O3-Fe1-O7	178.9(2)	O6-Fe2-O102	85.2(2)
O3-Fe1-O101	85.1(2)	O6-Fe2-O202	83.2(2)
O3-Fe1-O201	83.7(2)	O7-Fe2-O102	93.8(2)
O7-Fe1-O101	93.8(2)	O7-Fe2-O202	94.7(2)
O7-Fe1-O201	96.3(2)	O102-Fe2-O202	96.3(2)
O101-Fe1-O201	97.6(2)		

Intramolecular Distances (Å)

Fe1···Fe2	3.19 Å		
Fe1···C1	4.55 Å	Fe2···C7	4.00 Å
Fe1···C2	3.99	Fe2···C8	4.56
Fe1···C3	4.00	Fe2···C9	4.33
Fe1···C4	4.61	Fe2···C10	4.53
Fe1···C5	4.35	Fe2···C11	4.54
Fe1···C6	4.40	Fe2···C12	4.28

Table 2.5: Selected Bond Distances and Angles for **4**

Bond Distances (Å)			
Fe1-O1(hydroxo)	1.96 Å	Fe2-O1(hydroxo)	1.94 Å
Fe1-O2	2.04	Fe2-O5	2.00
Fe1-N3	2.08	Fe2-O18	2.00
Fe1-N5	2.07	Fe2-O10(water)	2.04
Fe1-O101	1.98	Fe2-O102	2.00
Fe1-O201	2.01	Fe2-O202	2.04

Bond Angles (deg)			
Fe1-O1-Fe2	124.1	O1-Fe2-O5	94.7
O1-Fe1-O2	94.7	O1-Fe2-O10	173.6
O1-Fe1-O101	89.8	O1-Fe2-O18	94.5
O1-Fe1-O201	90.3	O1-Fe2-O102	90.6
O1-Fe1-N3	94.5	O1-Fe2-O202	90.0
O1-Fe1-N5	87.2	O5-Fe2-O10	88.1
O2-Fe1-O101	175.5	O5-Fe2-O18	92.5
O2-Fe1-O201	85.0	O5-Fe2-O102	173.9
O2-Fe1-N3	89.3	O5-Fe2-O202	85.8
O2-Fe1-N5	88.1	O10-Fe2-O18	91.1
O101-Fe1-O201	95.2	O10-Fe2-O102	87.0
O101-Fe1-N3	90.2	O10-Fe2-O202	84.5
O101-Fe1-N5	87.3	O18-Fe2-O102	84.0
O201-Fe1-N3	172.8	O18-Fe2-O202	175.3
O201-Fe1-N5	89.7	O102-Fe2-O202	97.2
N3-Fe1-N5	85.8		

Intramolecular Distances (Å)			
Fe1···Fe2	3.45	O1···O3	2.80
O10···O19(water)	2.54	O1···O7	2.79

Table 2.6. Final Atom Positional and Equivalent Isotropic Thermal Parameters for $[Fe_2O(XDK)(DMSO)_6](NO_3)_2 \cdot 2DMSO \cdot Me_2CO \cdot H_2O$, $3 \cdot 2DMSO \cdot Me_2CO \cdot H_2O$.[a]

atom	x	y	z	B(eq)[b]
Fe(1)	0.88768(8)	0.22932(8)	0.19014(7)	1.32(3)
Fe(2)	0.90656(9)	0.04719(8)	0.19179(7)	1.60(3)
S(1)	0.7306(2)	0.1557(2)	0.0185(1)	2.25(5)
S(2)	1.0255(2)	0.3978(2)	0.1313(2)	2.52(5)
S(3)	0.9424(2)	0.4039(2)	0.3454(1)	2.62(5)
S(4)	0.7652(2)	-0.1664(2)	0.1089(2)	3.03(6)
S(5)	1.0672(2)	-0.0229(2)	0.1339(2)	3.52(7)
S(6)	0.9940(2)	0.0008(1)	0.3507(1)	2.23(5)
S(401)	0.5620(3)	0.3255(2)	0.2372(2)	6.2(1)
S(402)	0.567(1)	0.4658(9)	0.8610(8)	18.0(4)
S(403)	0.5035(8)	0.4215(7)	0.8509(6)	2.5(2)
O(1)	0.7481(4)	0.2005(3)	0.1120(3)	1.9(1)
O(2)	0.9569(4)	0.2935(4)	0.1067(3)	2.3(1)
O(3)	0.8986(4)	0.3568(3)	0.2510(3)	1.9(1)
O(4)	0.7723(4)	-0.0712(3)	0.1198(4)	2.4(1)
O(5)	0.9819(4)	0.0026(4)	0.1088(3)	2.5(1)
O(6)	0.9363(4)	-0.0335(3)	0.2581(3)	2.0(1)
O(7)	0.8805(4)	0.1196(3)	0.1389(3)	1.7(1)
O(101)	1.0332(4)	0.2797(4)	0.2662(3)	1.8(1)
O(102)	1.0483(4)	0.1517(3)	0.2653(3)	1.8(1)
O(103)	1.1685(4)	0.4472(4)	0.4581(4)	2.5(1)
O(104)	1.2086(4)	0.1967(4)	0.4660(4)	2.7(2)
O(201)	0.8048(4)	0.1866(4)	0.2744(3)	1.7(1)
O(202)	0.8229(4)	0.0620(3)	0.2789(3)	1.6(1)
O(203)	0.8159(4)	0.2999(4)	0.4825(4)	2.7(2)
O(204)	0.8468(4)	0.0419(4)	0.4740(4)	2.1(1)
O(401)	0.3292(9)	0.0492(8)	0.2616(8)	11.0(4)
O(402)	0.309(1)	-0.0671(8)	0.1797(6)	10.2(4)
O(403)	0.3457(8)	-0.0477(7)	0.3076(6)	9.0(3)
O(404)	0.1739(9)	0.4292(7)	0.8641(6)	9.2(4)
O(405)	0.115(2)	0.298(1)	0.8365(10)	19.8(7)
O(406)	0.2392(9)	0.3634(8)	0.9296(7)	9.8(4)
O(407)	0.4854(7)	0.3599(6)	0.2230(7)	8.7(3)
O(408)	0.5374(8)	0.3761(8)	0.8978(7)	10.2(3)
O(410)	0.7142(6)	0.4056(5)	0.9964(5)	6.1(2)
O(411)	0.777(1)	0.3975(9)	0.7736(8)	12.4(5)
N(101)	1.1866(5)	0.3199(4)	0.4567(4)	1.9(2)
N(201)	0.8296(5)	0.1707(4)	0.4795(4)	1.6(2)
N(401)	0.3255(7)	-0.0242(7)	0.2491(7)	3.8(2)
N(402)	0.194(1)	0.373(1)	0.8748(7)	9.3(5)

38

Table 2.6 contd. Final Atom Positional and Equivalent Isotropic Thermal Parameters for $3 \cdot 2DMSO \cdot Me_2CO \cdot H_2O$.[a]

atom	x	y	z	B(eq)[b]
C(1)	0.6339(8)	0.1806(6)	-0.0277(6)	3.3(2)
C(2)	0.6518(6)	0.0350(6)	-0.0005(5)	2.5(2)
C(3)	0.9399(8)	0.4430(7)	0.1039(7)	4.3(3)
C(4)	1.0894(9)	0.4093(7)	0.0479(7)	4.4(3)
C(5)	1.0416(8)	0.5148(6)	0.3515(7)	4.6(3)
C(6)	0.849(1)	0.4370(8)	0.3756(7)	5.5(4)
C(7)	0.7044(8)	-0.2056(7)	0.1859(7)	4.4(3)
C(8)	0.6598(8)	-0.2364(6)	0.0195(6)	4.6(3)
C(9)	1.019(1)	-0.139(1)	0.076(1)	10.3(5)
C(10)	1.1586(9)	0.0185(9)	0.0760(7)	5.4(4)
C(11)	0.9286(7)	-0.0952(6)	0.3867(6)	2.9(2)
C(12)	1.1105(7)	-0.0083(6)	0.3483(6)	3.2(2)
C(101)	1.0844(6)	0.2348(6)	0.2671(5)	1.5(2)
C(102)	1.2135(6)	0.4025(5)	0.4385(5)	1.9(2)
C(103)	1.2331(6)	0.2618(6)	0.4394(5)	2.0(2)
C(104)	1.1827(7)	0.2576(6)	0.1623(6)	3.0(2)
C(105)	1.3543(7)	0.5366(6)	0.4159(7)	4.0(3)
C(106)	1.3907(6)	0.2517(7)	0.4154(6)	3.1(2)
C(107)	1.1979(6)	0.2830(6)	0.2597(5)	2.0(2)
C(108)	1.2487(6)	0.3889(6)	0.2957(6)	2.4(2)
C(109)	1.2984(6)	0.4300(6)	0.3912(6)	2.5(2)
C(110)	1.3738(6)	0.3934(6)	0.4146(6)	2.7(2)
C(111)	1.3150(6)	0.2882(6)	0.3921(6)	2.2(2)
C(112)	1.2669(6)	0.2471(6)	0.2970(6)	2.4(2)
C(201)	0.7743(6)	0.1080(5)	0.2843(5)	1.6(2)
C(202)	0.7895(6)	0.0751(6)	0.4636(5)	1.7(2)
C(203)	0.7718(6)	0.2170(6)	0.4671(5)	1.8(2)
C(204)	0.5984(6)	0.0165(6)	0.2012(5)	2.4(2)
C(205)	0.6389(7)	-0.0679(6)	0.4629(6)	3.1(2)
C(206)	0.6059(7)	0.2204(7)	0.4682(6)	3.1(2)
C(207)	0.6609(6)	0.0601(6)	0.2935(5)	1.8(2)
C(208)	0.6412(6)	-0.0156(5)	0.3342(5)	1.9(2)
C(209)	0.6714(6)	0.0167(5)	0.4308(5)	2.0(2)
C(210)	0.6195(6)	0.0763(6)	0.4639(6)	2.5(2)
C(211)	0.6543(6)	0.1590(6)	0.4334(5)	1.9(2)
C(212)	0.6272(6)	0.1306(6)	0.3388(5)	2.1(2)
C(301)	1.0080(6)	0.2445(6)	0.4695(5)	1.9(2)
C(302)	1.1122(6)	0.2992(6)	0.5099(5)	2.0(2)
C(303)	1.1487(6)	0.3350(6)	0.5945(5)	2.2(2)
C(304)	1.0770(7)	0.3175(6)	0.6428(5)	2.3(2)
C(305)	0.9710(6)	0.2615(5)	0.6055(5)	1.9(2)

Table 2.6 contd. Final Atom Positional and Equivalent Isotropic Thermal Parameters for $3 \cdot 2DMSO \cdot Me_2CO \cdot H_2O$.[a]

atom	x	y	z	B(eq)[b]
C(306)	0.9386(6)	0.2266(5)	0.5201(5)	1.6(2)
C(307)	1.2620(7)	0.3925(6)	0.6383(6)	3.7(2)
C(308)	0.8947(7)	0.2442(7)	0.6596(6)	3.4(2)
C(401)	0.4980(9)	0.2054(8)	0.1801(8)	6.0(4)
C(402)	0.6475(9)	0.3600(8)	0.1705(8)	6.7(4)
C(403)	0.471(2)	0.505(2)	0.905(1)	14.1(8)
C(404)	0.496(2)	0.409(2)	0.756(2)	13.9(9)
C(409)	0.645(3)	0.532(3)	0.875(2)	5.5(8)
C(410)	0.7343(9)	0.3196(7)	0.7623(9)	4.7(3)
C(411)	0.802(1)	0.3043(10)	0.842(1)	10.2(5)
C(412)	0.631(1)	0.254(1)	0.747(1)	10.9(6)

[a] Numbers in parentheses are errors in the last significant digit. [b] B(eq) = $4/3[a^2\beta_{11} + b^2\beta_{22} + c^2\beta_{33} + 2ab \cos(\gamma)\beta_{12} + 2ac \cos(\beta)\beta_{13} + 2bc \cos(\alpha)\beta_{23}]$.

Table 2.7. Final Atom Positional and Equivalent Isotropic Thermal Parameters for [Fe$_2$(OH)(XDK)(BIPhMe)(H$_2$O)(NO$_3$)$_3$]·5H$_2$O·0.5CH$_2$Cl$_2$, 4·5H$_2$O·0.5CH$_2$Cl$_2$.[a]

atom	x	y	z	B(eq)[b]
Fe(1)	0.3518(1)	0.0169(1)	0.33111(7)	1.99(6)
Fe(2)	0.2107(1)	0.0785(1)	0.28973(8)	2.32(6)
Cl(1)	0.4370(9)	0.137(1)	0.1122(7)	13.9(7)
Cl(3)	0.468(1)	0.256(2)	0.1811(10)	21(1)
O(1)	0.2762(4)	0.0336(6)	0.2823(3)	2.0(3)
O(2)	0.3968(5)	0.0689(7)	0.2996(4)	3.3(3)
O(3)	0.3416(7)	0.0420(9)	0.2314(4)	5.5(5)
O(4)	0.4192(7)	0.1075(9)	0.2470(5)	6.2(5)
O(5)	0.1874(5)	0.1451(7)	0.2358(4)	3.8(4)
O(6)	0.1662(7)	0.1773(9)	0.1680(5)	6.8(5)
O(7)	0.212(1)	0.074(2)	0.1939(9)	5.1(7)
O(8)	0.241(1)	0.113(2)	0.2042(9)	4.3(6)
O(9)	0.4791(5)	-0.1949(6)	0.3880(4)	2.9(3)
O(10)	0.1483(4)	0.1308(6)	0.3039(3)	2.7(3)
O(18)	0.1561(7)	-0.0048(9)	0.2564(5)	6.6(4)
O(19)	0.1725(7)	0.1746(9)	0.3832(5)	7.4(5)
O(20)	0.0936(7)	-0.065(1)	0.2004(6)	7.6(5)
O(21)	0.085(1)	0.060(2)	0.2092(9)	7.0(7)
O(22)	0.165(2)	-0.011(2)	0.203(1)	5.8(9)
O(24)	0.0437(6)	0.072(2)	0.2918(7)	14.5(9)
O(26)	0.174(2)	0.101(3)	0.050(2)	8(1)
O(27)	0.258(1)	0.129(2)	0.1146(10)	8.8(9)
O(30)	0.109(2)	0.092(3)	0.048(2)	10(1)
O(33)	0.307(2)	0.123(2)	0.126(1)	6(1)
O(35)	0.327(3)	0.140(4)	0.106(2)	10(1)
O(101)	0.3141(5)	-0.0353(7)	0.3656(3)	2.6(3)
O(102)	0.2252(5)	0.0113(7)	0.3426(3)	2.5(3)
O(103)	0.3638(5)	-0.0435(7)	0.4802(4)	3.1(3)
O(104)	0.1789(5)	0.0383(7)	0.4260(4)	3.5(3)
O(201)	0.3488(5)	0.1221(6)	0.3550(3)	2.3(3)
O(202)	0.2607(5)	0.1688(6)	0.3231(3)	2.2(3)
O(203)	0.4293(5)	0.2042(7)	0.4611(4)	3.0(3)
O(204)	0.2482(5)	0.2957(7)	0.4015(4)	2.8(3)
N(1)	0.3846(8)	0.0720(10)	0.2581(6)	3.9(5)
N(2)	0.1931(7)	0.1369(10)	0.2004(5)	4.0(5)
N(3)	0.3653(6)	-0.0886(8)	0.3073(4)	2.1(3)
N(4)	0.4008(6)	-0.1938(8)	0.2934(5)	2.7(4)
N(5)	0.4294(5)	-0.0029(7)	0.3843(4)	2.2(3)
N(6)	0.5118(5)	-0.0469(8)	0.4310(4)	2.3(3)
N(9)	0.121(1)	-0.009(2)	0.2179(8)	9.0(7)
N(101)	0.2714(6)	-0.0054(7)	0.4527(4)	2.1(3)
N(201)	0.3391(6)	0.2463(8)	0.4282(4)	2.0(3)

Table 2.7 contd. Final Atom Positional and Equivalent Isotropic Thermal Parameters for $4 \cdot 5H_2O \cdot 0.5CH_2Cl_2$.[a]

atom	x	y	z	B(eq)[b]
C(1)	0.4095(7)	-0.1335(10)	0.3218(5)	2.2(4)
C(2)	0.3263(7)	-0.120(1)	0.2687(5)	2.4(4)
C(3)	0.3469(7)	-0.184(1)	0.2600(5)	2.4(4)
C(4)	0.4399(9)	-0.263(1)	0.2962(7)	4.8(6)
C(5)	0.4672(7)	-0.0585(9)	0.3917(5)	1.8(4)
C(6)	0.4508(8)	0.046(1)	0.4201(6)	3.3(5)
C(7)	0.5013(8)	0.020(1)	0.4486(5)	3.4(5)
C(8)	0.5644(8)	-0.093(1)	0.4527(6)	3.9(5)
C(9)	0.4666(7)	-0.1258(9)	0.3621(5)	2.2(4)
C(10)	0.4380(8)	-0.211(1)	0.4062(6)	3.5(4)
C(11)	0.5160(7)	-0.1164(9)	0.3470(5)	1.7(3)
C(12)	0.5143(8)	-0.050(1)	0.3223(6)	3.0(4)
C(13)	0.5558(9)	-0.036(1)	0.3060(7)	4.6(5)
C(14)	0.6024(9)	-0.086(1)	0.3172(7)	4.9(5)
C(15)	0.6041(9)	-0.153(1)	0.3424(7)	5.0(5)
C(16)	0.5616(8)	-0.167(1)	0.3581(6)	3.8(4)
C(101)	0.2639(9)	-0.0418(10)	0.3601(5)	2.4(5)
C(102)	0.3137(8)	-0.061(1)	0.4634(5)	2.4(5)
C(103)	0.2127(8)	-0.016(1)	0.4344(5)	2.6(5)
C(104)	0.2273(8)	-0.166(1)	0.3232(6)	3.4(5)
C(105)	0.3381(9)	-0.199(1)	0.4859(6)	4.0(5)
C(106)	0.1312(10)	-0.111(1)	0.4232(6)	5.6(7)
C(107)	0.2419(8)	-0.122(1)	0.3687(5)	2.6(5)
C(108)	0.2876(8)	-0.1641(10)	0.4066(5)	2.8(5)
C(109)	0.2936(8)	-0.144(1)	0.4538(6)	2.6(5)
C(110)	0.2358(9)	-0.156(1)	0.4549(5)	3.4(5)
C(111)	0.1922(8)	-0.102(1)	0.4232(6)	2.8(5)
C(112)	0.1853(8)	-0.119(1)	0.3753(6)	3.4(5)
C(201)	0.3156(8)	0.174(1)	0.3381(5)	2.4(5)
C(202)	0.3968(8)	0.247(1)	0.4339(5)	2.4(4)
C(203)	0.2954(8)	0.2990(9)	0.4027(5)	2.0(4)
C(204)	0.3331(8)	0.243(1)	0.2809(6)	3.1(5)
C(205)	0.4779(8)	0.321(1)	0.4300(6)	3.7(5)
C(206)	0.2775(8)	0.429(1)	0.3711(6)	3.8(5)
C(207)	0.3378(7)	0.253(1)	0.3290(5)	2.5(4)
C(208)	0.4015(7)	0.265(1)	0.3601(5)	2.6(5)
C(209)	0.4131(7)	0.303(1)	0.4065(5)	2.4(4)
C(210)	0.3794(8)	0.375(1)	0.4003(5)	2.9(5)
C(211)	0.3134(7)	0.3584(10)	0.3771(5)	2.3(4)
C(212)	0.3021(7)	0.3232(10)	0.3308(6)	2.9(5)

Table 2.7 contd. Final Atom Positional and Equivalent Isotropic Thermal Parameters for $4 \cdot 5H_2O \cdot 0.5CH_2Cl_2$.[a]

atom	x	y	z	B(eq)[b]
C(301)	0.3051(5)	0.1212(7)	0.4412(3)	4.4569
C(302)	0.2892(5)	0.0718(5)	0.4676(4)	4.4569
C(303)	0.2914(5)	0.0969(6)	0.5084(4)	4.4569
C(304)	0.3094(5)	0.1716(7)	0.5229(3)	4.4569
C(305)	0.3252(5)	0.2210(5)	0.4965(4)	4.4569
C(306)	0.3231(5)	0.1959(6)	0.4556(4)	4.4569
C(307)	0.2771(8)	0.043(1)	0.5390(5)	3.0(5)
C(308)	0.3479(8)	0.301(1)	0.5129(5)	3.4(5)
C(401)	0.460(2)	0.166(3)	0.158(2)	8(1)
C(402)	0.037(2)	0.076(3)	0.336(2)	5(1)

[a] Numbers in parentheses are errors in the last significant digit. [b] $B(eq) = 4/3[a^2\beta_{11} + b^2\beta_{22} + c^2\beta_{33} + 2ab\,\cos(\gamma)\beta_{12} + 2ac\,\cos(\beta)\beta_{13} + 2bc\,\cos(\alpha)\beta_{23}]$.

Table 2.8: Crystallographic Information for Complex **2**

Compound	$2 \cdot Tl(BF_4) \cdot 2CH_3OH^a$
Formula	$C_{46}H_{76}N_8O_{11}BF_4Fe_2Tl$
Formula Weight, g/mol	1531.49
Crystal Size, mm	not measured[b]
Crystal System	orthorhombic
Space Group	Pnnm
a, Å	33.75(2)
b, Å	12.61(1)
c, Å	17.02(1)
Volume, $Å^3$	7245(8)
Z	4^c
Density (calc.), g/cm^3	1.58
Temperature, K	183.5
Abs. coeff., cm^{-1}	28.47
Trans. coeff., min/max	1.000- 1.000
2θ Range, deg	$3 < 2\theta < 45$
Index Range	+h, +k, +l
No. of data collected	5293
p-factor	0.030
R_{av}	0.00
No. of independent data	5293
No. of obs. unique data	1556
No. of parameters	203
Data/parameter ratio	7.7
R	13.5
R_w	15.7
GOF	2.54
Largest shift/esd	2.57

a This composition is an estimate based on what could be seen in the lattice. Elemental analysis was not obtained. b The crystal broke apart after data collection as measurement was being attempted. c The Fe-O-Fe plane sits on a mirror plane, so the asymmetric unit is actually half of the molecule.

Note: Because the crystal quality was low, resulting in very little observed data, a fully refined solution was not attempted.

**Table 2.9.** Unit cell Parameters, [Fe$_2$O(XDK)(tacn)(BIPhMe)(H$_2$O)](ClO$_4$)$_2$, 5(ClO$_4$)$_2$

Compound	5(ClO$_4$)$_2$·4DMF
Formula	C$_{66}$H$_{101}$N$_{13}$O$_{23}$Cl$_2$Fe$_2$
Formula Weight, g/mol	1627.2
Crystal Size, mm	0.3 x 0.23 x 0.1
Crystal System	orthorhombic
Space Group	P 222(#16)
a, Å	16.82(2)
b, Å	26.90(2)
c, Å	38.25(2)
α, deg	90.00
β, deg	90.00
γ, deg	90.00
Volume, Å^3	17310(33)
Z	8

The structure was unsolvable, due to the poor quality of the data (e.g., R(int) = 0.11)

45
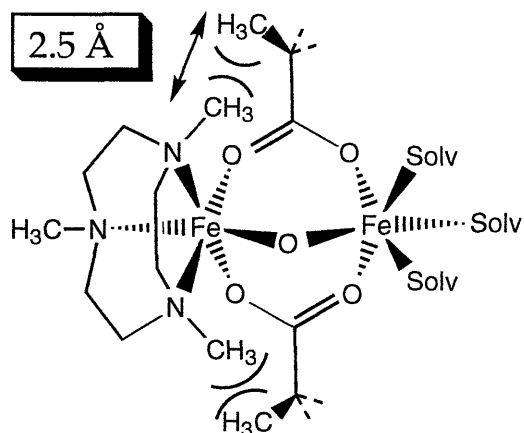
Figure 2.4: Results of CAChE Computer Modeling of Me₃tacn Bound to [Fe₂O(XDK)]²⁺
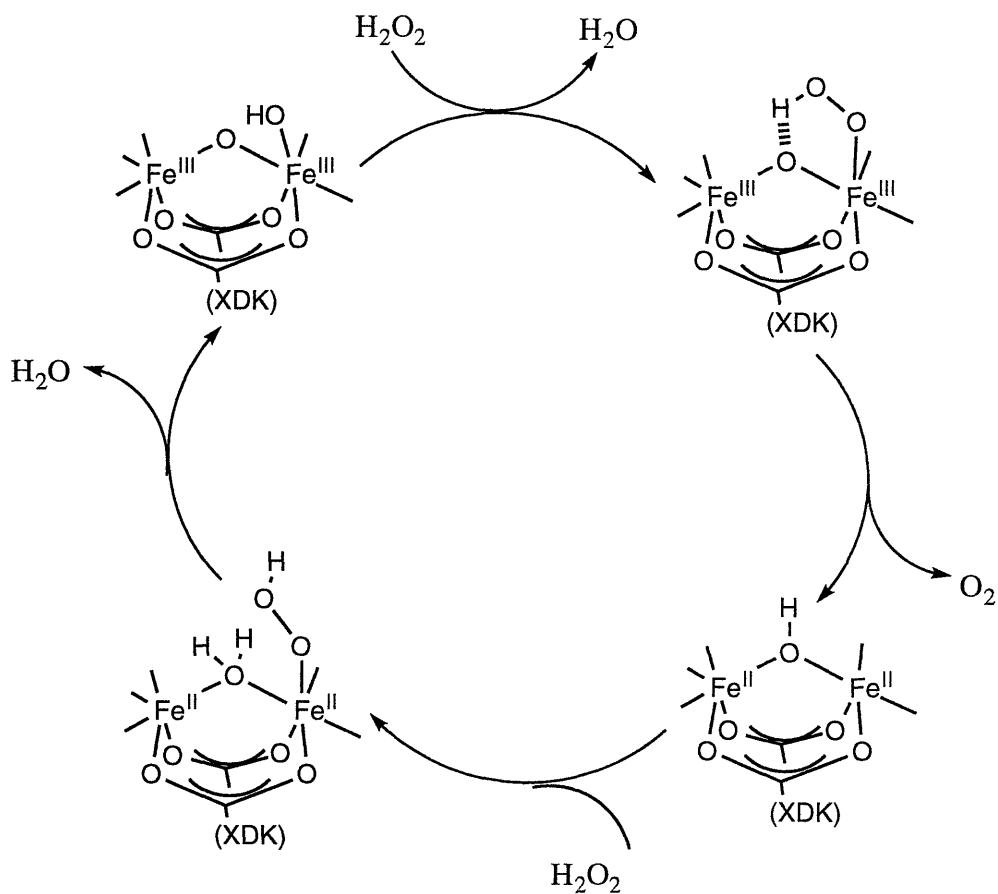
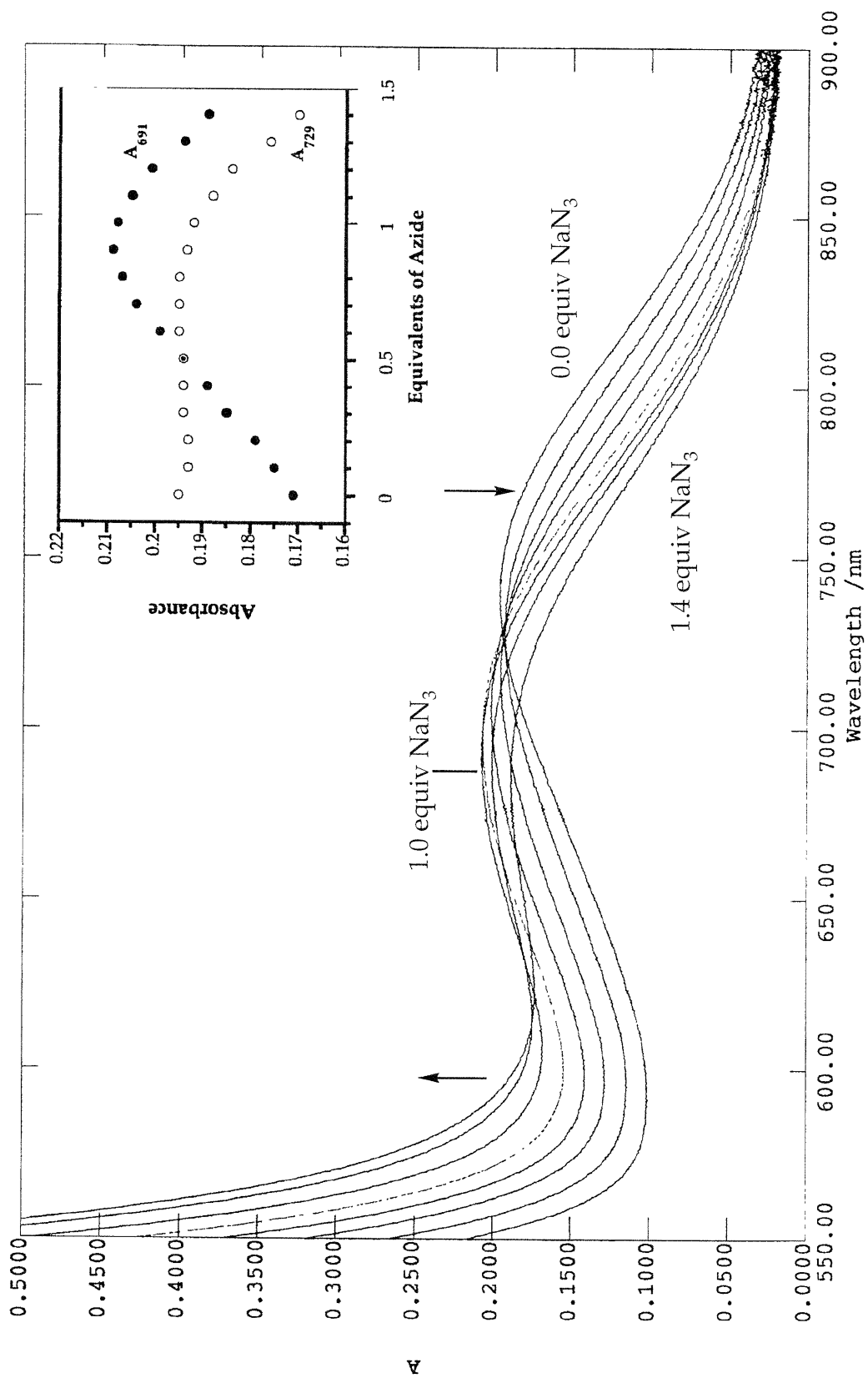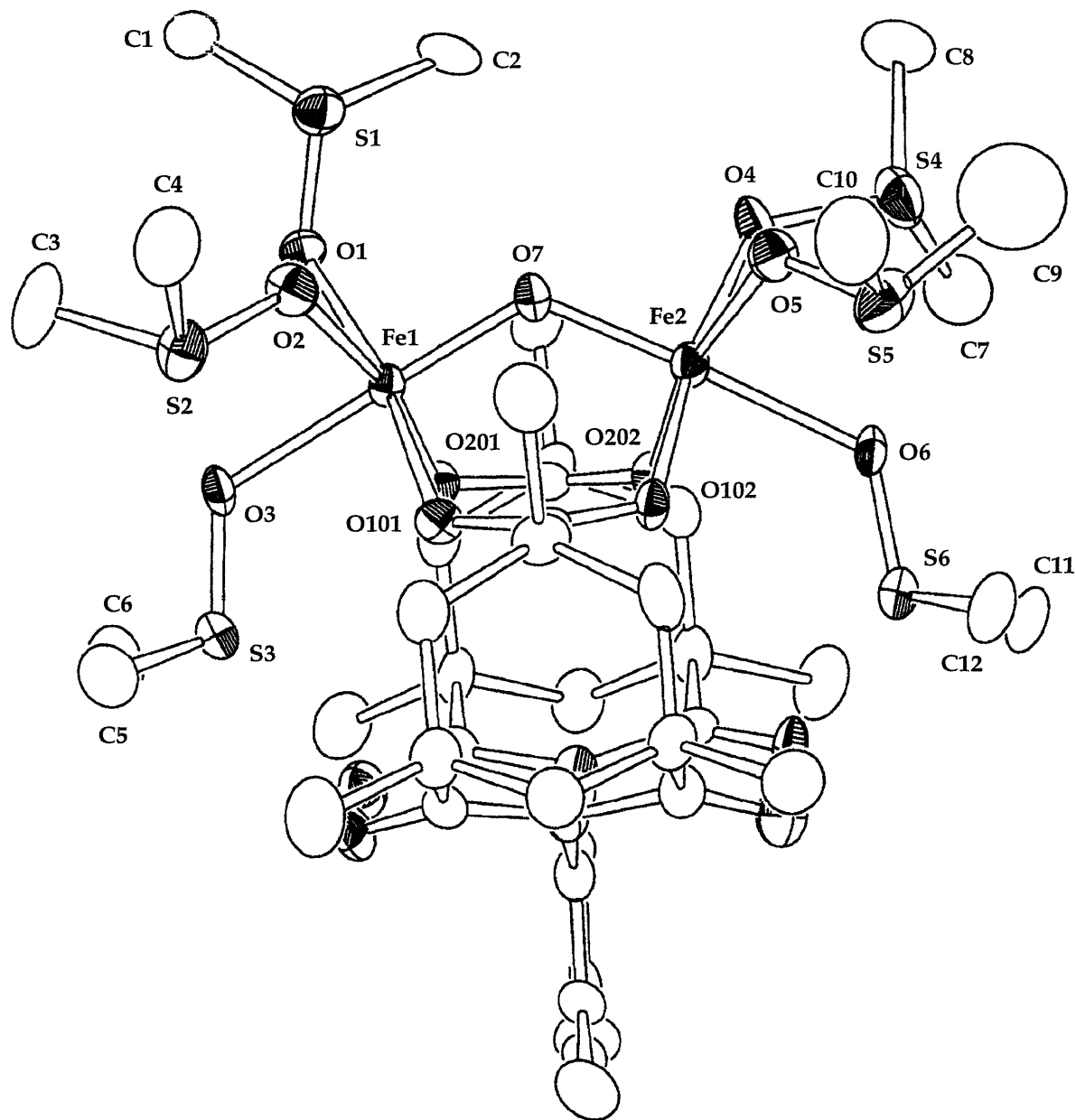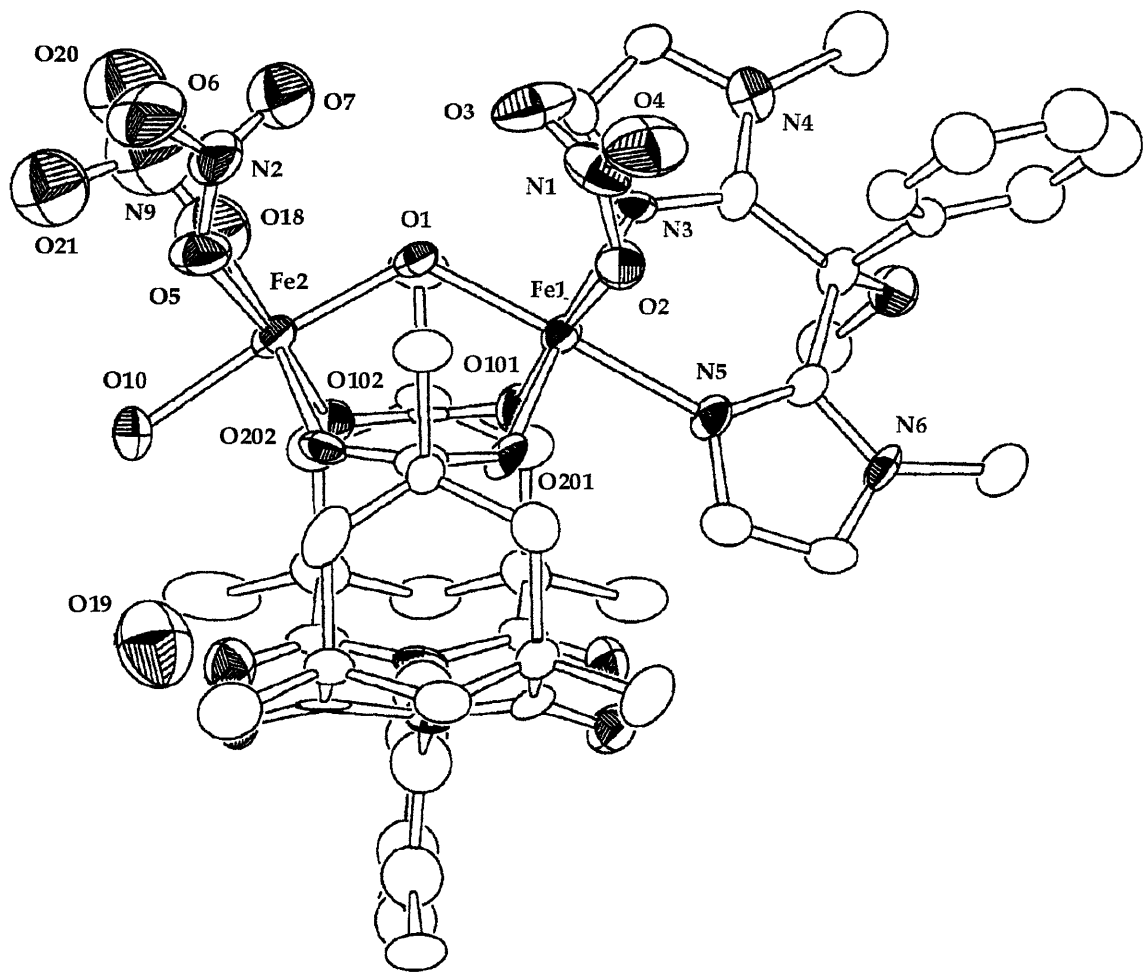**Figure 2.5:** Proposed mechanism for catalase activity of complex **5**, based on known reactions of hemerythrin.

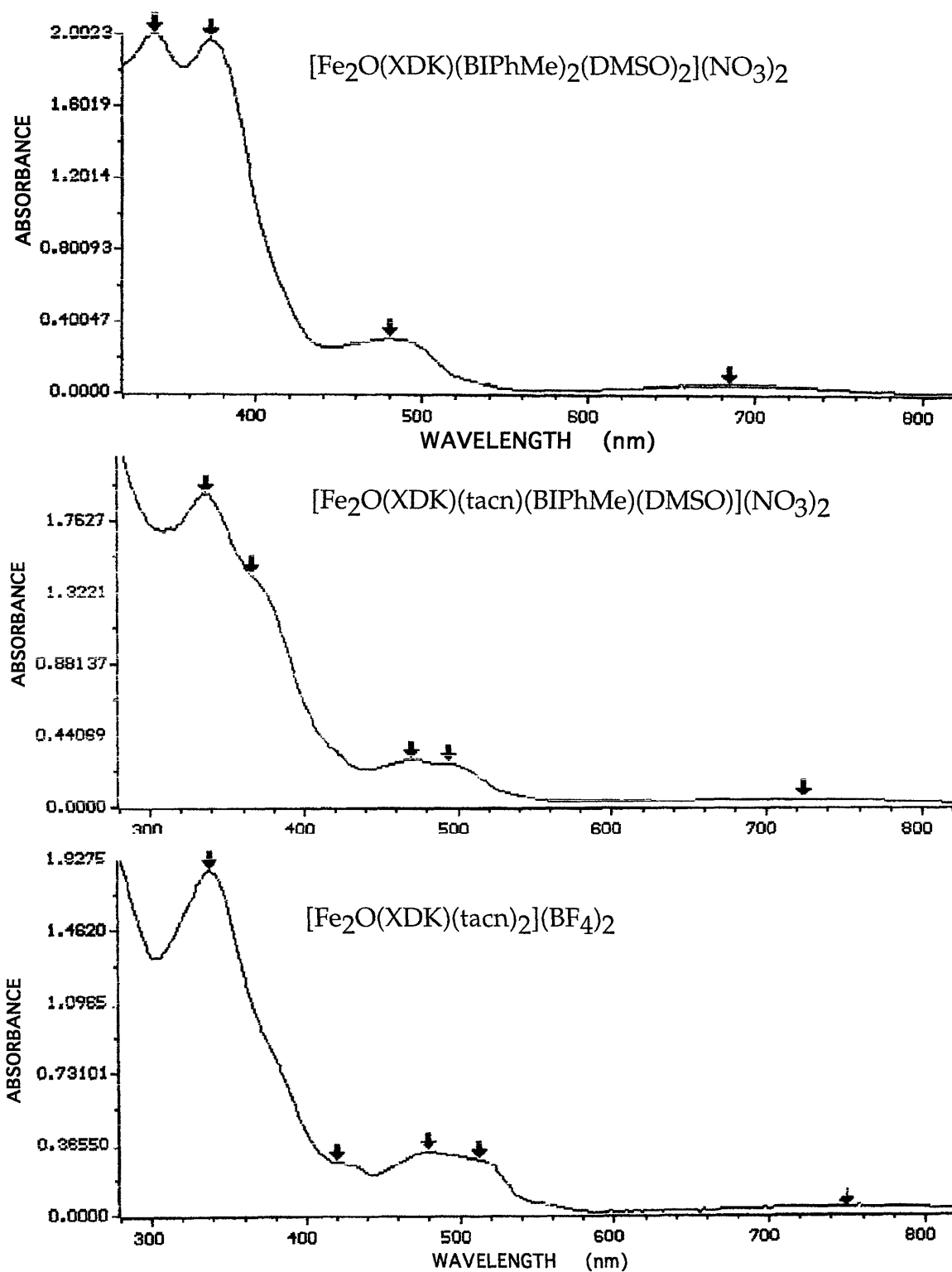**Figure 2.6:** Titration of complex **5** with 0.0 -1.4 equiv of NaN_3

Figure 2.7: ORTEP diagram of the cation in **3**, [Fe$_2$O(XDK)(DMSO)$_6$]$^{2+}$, showing 50% probability thermal ellipsoids for all non-hydrogen atoms.

Figure 2.8: ORTEP diagram of compound **4**, [Fe$_2$(OH)(XDK)(BIPhMe)(H$_2$O)(NO$_3$)$_3$], showing 50% probability thermal ellipsoids for all non-hydrogen atoms.

Figure 2.9: UV/visible spectra of Diiron(III) Complexes, showing the changes that occur as the number of nitrogen donor atoms is increased. Arrows mark the positions of absorption maxima or shoulders.

Chapter 3

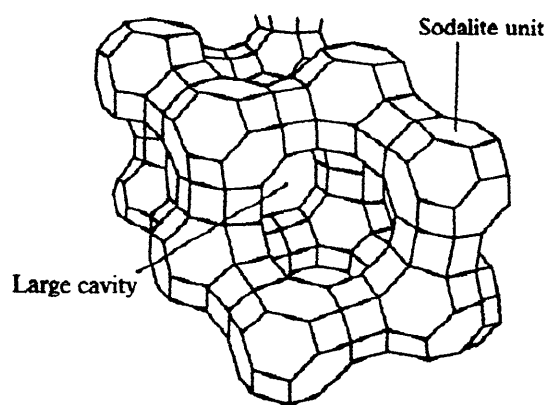# Zeolite-Encapsulated Iron Complexes

Introduction

A great deal of interest has arisen in recent years in mimicking the activity of non-heme iron metalloenzymes. These proteins catalyze a number of important oxidation reactions with dioxygen, including the hydroxylation of methane by methane monooxygenase,[1] ring cleavage by extradiol catechol dioxygenase,[2] and the generation of a tyrosyl radical by the iron center in ribonucleotide reductase.[3] In the biological systems, the protein framework is often responsible for the selectivity of the enzyme, and also protects reactive intermediates formed at the metal active site, preventing their decomposition by bimolecular pathways involving other metal complexes. Most model complexes lack such a protective sheath, with the result that bimolecular decomposition can often inactivate a small complex which might otherwise exhibit biomimetic oxidation activity.

One promising method for replicating the effect of the protein framework is to encapsulate a model compound inside a zeolite or clay. Model complexes contained in the large cavities of a zeolite are immobilized if they are too large to diffuse through the smaller pores, and the zeolite lattice can also impart some shape selectivity. This strategy has been successfully applied to metalloporphyrins and metallophthalocyanines in zeolite Y.[4] The traditional way that iron phthalocyanines (FePc) have been prepared inside zeolite Y is by a template synthesis where dicyanobenzenes are allowed to react with Fe^{2+}-exchanged zeolite Y. Increased catalytic turnover was observed for the zeolite-encapsulated complexes in the oxidation of hydrocarbons, and smaller substrates were selectively oxidized over larger hydrocarbons.[4,5] Even better results were obtained by embedding FePc-Y in a polydimethylsiloxane membrane, producing an efficient mimic of cytochrome P-450.[6] In general, turnover number was

higher when the loading of complex in the zeolite was low, resulting in less pore blockage.[4,5]

Zeolites are also capable of stabilizing catalytically active metal centers without the use of any external ligands. Metal ions such as titanium can be incorporated into the lattice, turning the zeolite into a catalyst for the oxidation of a range of hydrocarbons by hydrogen peroxide.[7] A similar example is the zeolite FeZSM-5, in which some of the irons move out of the lattice during calcination, forming iron oxide complexes that are proposed to be dinuclear.[8] This material can use N_2O catalytically to convert benzene to phenol or to oxidize methane stoichiometrically.[9,10]

Figure 3.1: Faujasite

Up to now, there have been no published investigations of encapsulated iron complexes that did not involve porphyrin or porphyrin-like ligands, such as Fe^{III}(salen) complexes.[4,11] A major goal of the research described here is to encapsulate models of non-heme iron enzymes in a zeolite in the hope that new catalysts for hydrocarbon oxidation may be found. Studies in our laboratory have shown that the dioxygen adducts initially formed from many diferrous complexes decompose by bimolecular pathways.[12,13] Isolating complexes from each other in zeolite cages should increase the lifetimes of the diiron(III) peroxo

intermediates, possibly leading to more reactive intermediates through cleavage of the O-O bond.

The zeolite used in this research is an essentially pure silica version of faujasite and is relatively uncharged and hydrophobic compared to most zeolites. This neutrality should help to limit side reactions catalyzed by acid sites in the framework, allowing activity due to the encapsulated iron complexes themselves to be investigated. In addition, the hydrophobicity of the zeolite should aid in the uptake of hydrocarbon substrates. The difficulty in this work has been knowing whether or not a complex has been formed inside the zeolite. Partial success in forming complexes has been achieved, but in many cases it is unclear whether or not the iron atom is bound to the ligand. In addition, partial oxidation of cyclohexene with hydrogen peroxide has been observed with iron-containing faujasites, although this activity apparently does not require a ligand. The results described here suggest a degree of complexity in the behavior of ligands and metal ions in the faujasite, and a clear understanding of the nature and role of ligand complexes in the zeolite will require more detailed studies of these materials.

Experimental

General. The high-silica faujasite, a research sample from TOSOH, was a gift from Professor Marc Davis at the California Institute of Technology. It has a Si/Al ratio of 300 and contains 4.2×10^{20} supercages per gram. The supercages are 13 Å in diameter, and the pores between supercages are 7.5 Å in width.

Methanol used in ligand impregnation was dried over 4 Å molecular sieves. All other solvents were dried and distilled under nitrogen by standard procedures.

The ligands HPTP,[14] Me$_3$tacn,[15] and KHBpz$_3$,[16] and the iron complex [Fe$_2$(HPTP)(OBz)](BPh$_4$)$_2$[14] were prepared according to literature methods. Tetramethylammonium benzoate and 2-picolinic acid were purchased and used as received. Cyclohexene was refluxed over CaH$_2$ and distilled under argon.

Non-aqueous hydrogen peroxide was prepared by vacuum distillation of water from 50% aqueous H$_2$O$_2$ into a flask cooled with liquid nitrogen. Volume decreased from 15 mL to 5 mL during the distillation, leaving about 98% pure H$_2$O$_2$ in the distilling flask, which was diluted with 15 mL of dry, distilled acetonitrile. CAUTION: Pure hydrogen peroxide is an explosion hazard. The apparatus shoud be kept behind a blast shield until the H$_2$O$_2$ is diluted with solvent.

All iron-containing faujasites were prepared in a nitrogen-filled Vacuum Atmospheres dry box. Ligand impregnation procedures, up to the filtration step, were carried out under argon using standard Schlenk techniques.

Thermogravimetric analysis (TGA) was carried out by Kurt Kendall on a TA Instruments SDT-2960 in the laboratory of Professor Hanno zur Loye at MIT.

Solid State NMR. Solid state ^{13}C spectra were collected on a Unity 300 MHz instrument with a Magic Angle Spinning (MAS) probe. The spectra were cross-polarized with a pulse of 0.3 ms contact time and proton-decoupled. Samples were spun at 4.5 - 6 kHz during overnight acquisitions of ~10,000 transients.

Preparation of HPTP-FAU. A 0.50-g sample of TOSOH high-silica faujasite was activated by heating under vacuum at 100°C for 4 h. After cooling, a solution of 16 mg (3.5 x 10^{-5} mol; 1 ligand/10 supercages) of HPTP in MeOH (dried over molecular sieves) was added with enough MeOH to cover the faujasite, and the slurry was refluxed with vigorous stirring for 36 hours. The faujasite was then isolated by filtration and washed several times with MeOH,

stirred with fresh MeOH, and filtered and washed again. It was dried by heating under vacuum at 80°C for 2 h. A total of about 4 mg of HPTP was recovered from the washings, indicating that 12 mg (2.4% by weight) remained in the faujasite. Thermogravimetric analysis (TGA) of a portion of this material confirmed that approximately 2.2% of the sample weight was lost between 200°C and 600°C, presumably from combustion of the organic material. This level of loading corresponds to one ligand/14 supercages.

A higher loading of HPTP in the high-silica faujasite was also prepared by the same method by using 160 mg (0.35 mmol; 1 ligand/supercage) of HPTP and 0.50 g of faujasite in the methanol slurry. About 95 mg of ligand was recovered in the washings in this case, indicating that 65 mg (1 ligand/2.5 supercages) remained in the zeolite. An attempt to increase the loading even further by reactivating the partially impregnated faujasite and refluxing it for 5 days in MeOH with the remaining 95 mg of HPTP resulted in complete recovery of the excess ligand.

Preparation of [Fe$_2$(HPTP)]$^{3+}$-FAU. A 0.2-g sample of HPTP-FAU (1 ligand/14 supercages) was dried overnight at 80°C under vacuum and brought into a dry box. This material was mixed with a solution of 7 mg (2.1 x 10^{-5} mol; 1 Fe/7 supercages) of [Fe(H$_2$O)$_6$](BF$_4$)$_2$ in a minimal amount of MeOH and 1 mg (1 x 10^{-5} mol) of NEt$_3$. The resulting bright yellow slurry was stirred at room temperature overnight and filtered to isolate the yellow faujasite. The initial filtrate was also yellow, but subsequent MeOH washings were colorless. The bright yellow solid was dried in the atmosphere of the dry box. Anal. Calcd (based on 1 C$_{27}$H$_{29}$N$_6$/14 supercages): C 1.69%, H 0.17%, N 0.44%. Found: C 1.64%, H 0.28%, N 0.11%. Due to the small amount of organic material in the sample, substantial error is possible, especially for H and N.

Preparation of [Fe$_2$(HPTP)(OBz)]$^{2+}$-FAU. This Fe^{2+}-containing faujasite was prepared in the same way as [Fe$_2$(HPTP)]$^{3+}$-FAU, except that it was carried out on a 0.13-g scale of HPTP-FAU, and 1.1 mg (1 molecule/14 supercages) of tetramethylammonium benzoate was added to the slurry. The color of the resulting faujasite was identical to that of [Fe$_2$(HPTP)]$^{3+}$-FAU. Anal. Calcd for 1 C$_{34}$H$_{34}$N$_6$O$_3$/14 supercages: C 1.96%, H 0.16%, N 0.4%. Found: C 1.96%, H 0.42%, N <0.1%.

Preparation of Me$_3$tacn-FAU. To 0.50 g of activated TOSOH high-silica faujasite was added a solution of 16 mg (9.3 x 10^{-5} mol; 1 ligand/3.7 supercages) of Me$_3$tacn in 2 mL of MeOH. The slurry was refluxed with vigorous stirring for 2 d, and the faujasite was isolated by filtration and washed several times with MeOH. The white powder was dried at room temperature under vacuum. The washings contained about 3 mg of Me$_3$tacn, leaving 13 mg (1 ligand/4.6 supercages) in the zeolite. Anal. Calcd for 1 C$_9$H$_{21}$N$_3$/4.6 supercages: C 1.60%, H 0.31%, N 0.62%. Found: C 2.01%, H 0.32%, N <0.1%.

A higher loading of Me$_3$tacn in the faujasite was prepared by the same procedure and using 77 mg of Me$_3$tacn in the impregnation. In this case, 32 mg (one ligand/1.5 supercages) remained in the faujasite. This sample was prepared for use in solid state CPMAS-NMR.

Preparation of Fe(Me$_3$tacn)-FAU. To 250 mg of Me$_3$tacn-FAU (1 ligand/ 4.6 supercages) was added a solution of 14 mg (4.1 x 10^{-5} mol) of [Fe(H$_2$O)$_6$](BF$_4$)$_2$ in 2 mL of methanol. The slurry was stirred overnight, filtered, and washed with methanol, and the white solid was dried under vacuum at room temperature. The solvent was evaporated under vacuum to yield 12 mg of brown solid in air. If the Me$_3$tacn and Fe(II) remaining in the faujasite were present in a 1:1 stoichiometry, the concentration based on the amount of recovered material would be about one [Fe(Me$_3$tacn)(H$_2$O)$_3$]$^{2+}$ complex/6

supercages. Anal. Calcd (based on 1 $FeC_9H_{21}N_3$/6 supercages): C 1.26%, H 0.29%, N 0.49%, Fe 0.65%. Found (Desert Analytics): C 1.88%, H 0.09%, N 0.09%, Fe 0.03% (approx. 1 Fe/130 supercages).

A more concentrated sample was prepared for CPMAS-NMR by using 300 mg of Me$_3$tacn-FAU with a higher loading (1 ligand/1.5 supercages) and adding 44 mg (0.13 mmol; 1 Fe/1.6 supercages) of $[Fe(H_2O)_6](BF_4)_2$ in 2 mL of methanol. After stirring for 3 h at room temperature, the slurry was filtered, washed with MeOH, and dried under vacuum. Evaporation of solvent from the supernatant and washings yielded 35 mg of $[Fe(H_2O)_6](BF_4)_2$.

Preparation of Fe-FAU. After activating 300 mg of TOSOH high-silica faujasite by heating at 100°C under vacuum for 4 hours, the faujasite was brought into a dry box and stirred with a solution of 25 mg (7.4×10^{-5} mol; 1 Fe/3 super-cages) of $[Fe(H_2O)_6](BF_4)_2$ in 2 mL of MeOH for 3 hours. The faujasite was then filtered, washed with methanol, and dried under vacuum with moderate heating. Evaporation of the filtrate yielded 14 mg of $[Fe(H_2O)_6](BF_4)_2$, leading to an estimated concentration of 1 Fe/6.4 supercages. Anal. Calcd for 1 Fe/6.4 supercages: Fe 0.65%. Found (Desert Analytics): 0.05% (1 Fe/78 supercages).

Preparation of KHBpz$_3$-FAU. After activating 300 mg of TOSOH high-silica faujasite by heating at 100 °C under vacuum for 4 h, a solution of 52 mg (0.21 mmol; 1 ligand/supercage) of KHBpz$_3$ in 3 mL of dry THF was added and the slurry was heated at 50 °C for 24 h. The suspension was filtered, washed with THF and methanol, and the white powder was dried by heating under vacuum. Solvent was evaporated from the supernatant, yielding 31 mg of a white residue, which meant that 21 mg (1 ligand/2.5 supercages) remained in the faujasite. However, the ^{1}H-NMR spectrum of the residue in D_2O showed several pyrazole-containing products in addition to KHBpz$_3$, indicating partial decomposition of the ligand.

58

Preparation of Fe(HBpz3)⁺-FAU. To 200 mg of KHBpz$_3$-FAU was added 17.2 mg (5.1 x 10^{-5} mol; 1 Fe/2.7 supercages) of [Fe(H$_2$O)$_6$](BF$_4$)$_2$ in 2 mL of methanol. The slurry was stirred at room temperature overnight, and the faujasite was filtered out, washed with methanol, and dried under vacuum. The supernatant and washes were evaporated to yield 10.5 mg of solid, which turned red upon exposure to air. The IR spectrum of this residue did not show any KHBpz$_3$. Given that 6.5 mg of KBF$_4$ was expected as a side-product, it was estimated that 50% of the available iron was loaded into the faujasite.

Preparation of Fe(PA)-FAU. To 150 mg of Fe-FAU (1 Fe/3.5 supercages) was added 6.8 mg (5.5 x 10^{-5} mol; 1 ligand/1.9 supercages) of 2-picolinic acid (PA) in 2 mL of acetonitrile. The faujasite immediately turned a light orange color. The slurry was stirred for 3 h, and the faujasite was filtered, washed with acetonitrile and ether, and dried under vacuum. The solution phase was evaporated to yield of 5.5 mg of picolinic acid, as identified by ^{1}H-NMR spectrometry.

Assays for Oxidation Activity in Fe-containing Faujasites. All solutions and reaction mixtures were prepared in a dry box. Generally, a 25-mg sample of the faujasite being studied was mixed with 0.8 mL of a 0.097 M solution of cyclohexene and 1.0 mL of a 0.18 M solution of H$_2$O$_2$, all in acetonitrile. The reaction flask was then capped and brought out of the dry box, and the slurry was stirred at room temperature for 20-50 h. To observe the course of the reaction, a 0.5-mL aliquot was removed, mixed with an equal volume of solution containing methyl benzoate as an internal standard, and centrifuged to precipitate the zeolite. Products were analyzed by GC and GC/MS using a Hewlett Packard (HP) Model 5890 gas chromatograph with an FID detector for one column and an HP Model 5971A mass spectrometer interfaced to another column. Both columns were cross-linked methyl silicon capillary columns (HP-

1) with dimensions of 50 m x 0.2 mm x 0.5 µm. Typical conditions were as follows: initial temp., 40°C; initial time, 14 min; heating rate, 15°C/min; final temp., 190°C.

In other oxidation assays, the H_2O_2 solution was omitted and replaced either with solvent or a 94 mM solution of hydroquinone as reducing agent. After removal from the dry box, the atmosphere of the flask was purged with O_2 and stirred at least 24 h before being worked up as above.

Results and Discussion

Ligand Impregnation. The general approach taken in this work to the preparation of intrazeolitic iron complexes was to add a ferrous salt to a zeolite already impregnated with a ligand. In theory, this strategy aids the uptake of iron into the zeolite and can also promote the formation of ligand complexes, provided that the iron binds preferentially to the ligand rather than to other sites in the zeolite. For some ligands, this approach allows for a more even distribution of the ligand throughout the zeolite. Subsequent formation of a larger and more rigid iron complex traps the compound in a supercage, for it is now unable to diffuse through the pores of the zeolite.

Faujasite samples were impregnated with a ligand by refluxing a solution of the latter with the zeolite. Methanol was used most often in this procedure because of the solubility of all the ligands in this solvent. This method worked well for relatively nonpolar ligands such as HPTP and Me$_3$tacn. Loading efficiencies were 75% or greater for low attempted loadings of these two ligands, and about 40% at higher concentrations. Washing the impregnated faujasites with fresh methanol did not remove very much of the encapsulated ligand, implying that HPTP and Me$_3$tacn are absorbed in the hydrophobic interior of the faujasite, rather than adsorbed on the surface. In contrast, highly polar and

ionizable ligands such as 2-picolinic acid and HPTA could not be loaded to any significant extent in methanol, perhaps due to their preference for a polar environment. For picolinic acid, this problem was solved by adding ligand to an iron-containing faujasite, but HPTA proved too insoluble in methanol at room temperature or in less polar solvents for either approach to be feasible. Another ligand which could not be loaded into the faujasite was BIPhMe, although in this case the effective diameter (> 8 Å) and rigidity of the molecule may have prevented it from passing through the 7.5-Å pores.

HPTP

Me₃tacn

BIPhMe

KHBpz₃

HPTA

2-Picolinic acid
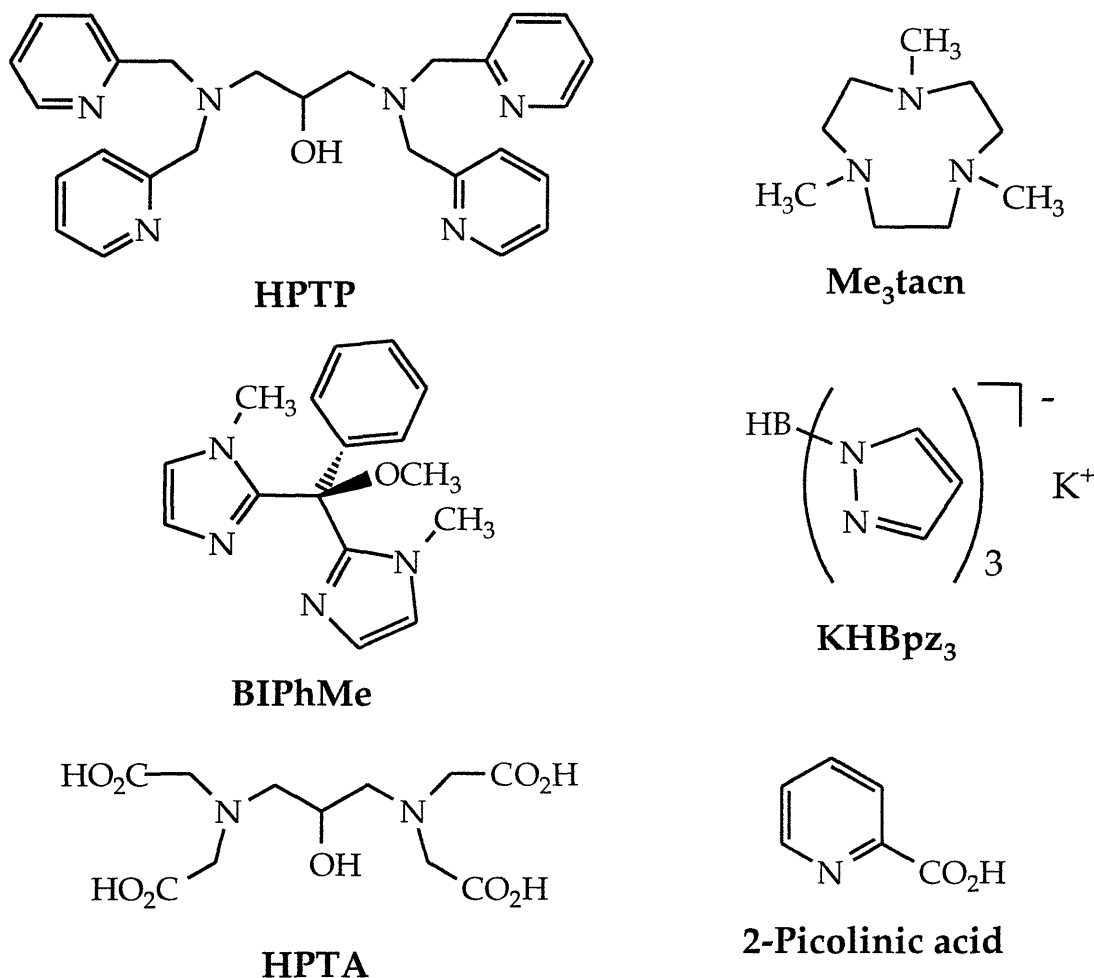
Figure 3.2: Ligands Used or Attempted for Impregnation

In the case of KHBpz$_3$, the ionic character of the compound was expected to hinder encapsulation inside the hydrophobic faujasite. Accordingly, the ligand impregnation was performed in THF to induce ion pairing. When the resulting KHBpz$_3$-FAU was stirred with methanol, less than 5% of the ligand could be washed out. It is not clear, however, whether the encapsulated molecules are intact, since free pyrazole and H$_2$Bpz$_2^-$ were observed in the NMR spectrum of the excess ligand left in solution (Figure 3.3).

Encapsulated Iron Complexes. According to the results of elemental analysis, very low loading levels of Fe^{2+}, around 1 Fe/100 supercages, were achieved in the preparation of Fe-FAU and Fe(Me$_3$tacn)-FAU, in contrast to much higher estimates based on the amount of material recovered. A control experiment in which a methanol solution of [Fe(H$_2$O)$_6$](BF$_4$)$_2$ was filtered and evaporated also showed the loss of 6 mg from a 13-mg sample, however, so the latter should be ignored. The actual loading of iron in Fe-FAU corresponds to 1 Fe/6 Al, or one-third the exchange capacity of the zeolite since there is one negative charge in the lattice per aluminum atom. Although the reported amount of iron in Fe(Me$_3$tacn)-FAU is even lower, the estimated error in the weight percent of iron ($\pm 0.01\%$) means that the loading in both Fe-FAU and Fe(Me$_3$tacn)-FAU may be nearly identical. It is likely that similar levels of iron will be found in the other Fe-containing faujasites.

The presence of a ligand in the faujasite clearly does not result in stoichiometric loading of iron into the zeolite. For example, when iron was added to the concentrated Me$_3$tacn-FAU, material equivalent to 80% of the stoichiometric amount of Fe^{2+} for a 1:1 complex was recovered in the washings. The results of elemental analysis for Fe(Me$_3$tacn)-FAU confirm that the presence of a ligand does not increase the loading of iron, even though the actual loading of the ligand may be lower than expected, too. These data indicate that, in at least

one case, interaction with a ligand is not a determining factor in the degree of iron loading attainable. Given that the actual loading is quite low, this conclusion may indicate that iron cations preferentially bind to the lattice of the faujasite, rather than the ligand.

In some cases, addition of the ferrous salt to a ligand-containing fauajsite did appear to result in formation of intrazeolitic complexes. For example, addition of Fe^{2+} to HPTP-FAU, with or without benzoate, resulted immediately in a bright yellow color, similar to the color of $[Fe_2(HPTP)(O_2CPh)](BF_4)_2$ in very dilute solutions. The yellow color was associated with the solid faujasite, and could not be washed out by acetonitrile or methanol, implying that the complexes were trapped inside the zeolite. Addition of 2-picolinic acid to Fe-FAU also produced a color change to orange, perhaps indicating formation of a complex with iron. In the cases of Me_3tacn and $KHBpz_3$, no color changes were observed upon addition of the ferrous salt to the ligand-containing faujasite, although Me_3tacn produces a colored complex when added to iron(II) in solution. Absence of color is not proof that complexes did not form, however, since the color may have been too weak to be visible.

Solid State NMR. Cross-polarized Magic Angle Spinning (MAS) NMR of ^{13}C nuclei in concentrated samples of HPTP-FAU (Figure 3.4) and Me_3tacn-FAU (Figure 3.5 A) gave spectra which were consistent with the presence of intact ligands in the materials (Table 3.2). The signals were significantly broadened due to the effect of the matrix, and possibly because limited mobility of the confined ligands led to inequivalence in carbon atoms with the same chemical shift which was not resolvable in these experiments. In the case of $KHBpz_3$-FAU, the spectrum obtained did not show any signals attributable to the ligand (Figure 3.6), despite a degree of loading similar to that of the HPTP-FAU sample studied. The

63

presence of a magnetic ^{11}B nucleus (S = 3/2) may have broadened the signals beyond our detection limits.

The solid state NMR spectrum of a concentrated sample of Fe(Me$_3$tacn)-FAU was also obtained (Figure 3.5 B). A signal corresponding to the ligand was observed again, but much weaker than it had been in the same material before addition of iron. A very broad feature centered around the Me$_3$tacn signals was also apparent, possibly arising from signals broadened by proximity to paramagnetic metal center. Although these data are inconclusive, the presence of both broadened and unbroadened signals is consistent with the substoichiometric amount of iron loaded into this sample.

Reactions with Dioxygen. Most of the iron-containing faujasites did not undergo any obvious changes when allowed to react with dioxygen. Visible changes were observed upon addition of dioxygen to slurries of [Fe$_2$(HPTP)]-FAU and [Fe$_2$(HPTP)(O$_2$CPh)]-FAU in acetonitrile. The former changed from yellow to a darker orange before bleaching to a pale yellow in less than a minute. In a similar fashion, [Fe$_2$(HPTP)(O$_2$CPh)]-FAU changed from yellow to greenish grey, and then bleached more gradually. As a reference, [Fe$_2$(HPTP)(O$_2$CPh)](BPh$_4$)$_2$ was prepared and allowed to react with dioxygen in solution, resulting in a change from orange to dark orange at room temperature.

The initial color change in [Fe$_2$(HPTP)]-FAU could be analogous to the solution behavior of the complex, although the final oxidation product in solution is known to be a tetranuclear species,[13] which is unlikely to form in the confined spaces of the zeolite. If the more intense color is due to interaction between iron(III) and the ligand, however, these visible changes may be exactly analogous. The initial green color observed in [Fe$_2$(HPTP)(O$_2$CPh)]-FAU is more tantalizing because of its similarity to the blue color of the known diiron(III)-peroxo complex, which in solution can only be observed at low temperature.[13,14]

Stabilization of the peroxo intermediate at room temperature in a zeolite would be noteworthy. Spectroscopic characterization of these materials, perhaps by diffuse reflectance, is required before any conclusions can be made about the nature these intermediates.
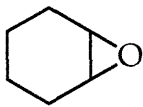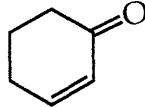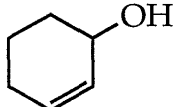
The reversion to a pale yellow by both materials after reaction with dioxygen could be an indication that the metal ions are no longer bound to the ligand. This bleaching has no precedent in the behavior of $[Fe_2(HPTP)(O_2CPh)]^{2+}$ in solution. Faujasite containing just HPTP exhibits the same pale yellow, whereas Fe-FAU is essentially colorless both before and after exposure to air. The implication is that, upon oxidation, sites associated with the lattice of the faujasite are thermodynamically favored over ligand sites. This conclusion is supported by the development of oxidation activity in the previously oxidized material, as described below. Oxidative degradation of the ligand might account for the apparent decomposition of the complex.

Reactions with Dioxygen and Substrate. All six Fe-containing faujasites were tested for oxidation of cyclohexene in the presence of dioxygen. Although in the presence of substrate $[Fe_2(HPTP)]$-FAU and $[Fe_2(HPTP)(O_2CPh)]$-FAU did not exhibit the intermediate color changes observed with only O_2, this difference in behavior did not translate into substrate oxidation. No products of cyclohexene oxidation were detected in any of the assays with O_2. Hydroquinone was added as a reducing agent in assays involving Fe-FAU and Fe(PA)-FAU, but benzoquinone was the only oxidized product detected in these runs (Figure 3.7).

Reaction with Hydrogen Peroxide and Substrate. When hydrogen peroxide was used, oxidation of cyclohexene to the epoxide, as well as some allylic oxidation, occurred in the presence of some Fe-containing faujasites. Dilute samples of Fe-FAU and Fe(Me$_3$tacn)-FAU exhibited similar levels of activity and identical product distributions, catalyzing 18-30 turnovers per iron

over the course of 20-40 h and converting about 5% of the substrate to product. Cyclohexene oxide represented 70-75% of the total yield of oxidized products, with 2-cyclohexen-1-one and 2-cyclohexen-1-ol making up the rest. No oxidation products were detected in the presence of faujasite without iron, and the epoxide was not formed in control experiments involving Fe^{2+} or $Fe(Me_3tacn)^{2+}$ and no faujasite. The Fe-containing faujasites $Fe(HBpz_3)$-FAU, $[Fe_2(HPTP)]$-FAU, and a previously oxidized sample of $[Fe_2(HPTP)]$-FAU also catalyzed oxidation of cyclohexene with H_2O_2, with higher amounts of the allylic oxidation products. Only Fe(PA)-FAU was inactive, generating only trace amounts of oxidized products. One run with cyclohexane as substrate and Fe-FAU as catalyst yielded no detectable products of alkane oxidation.

Table 3.1. Cyclohexene Oxidation with Various Fe-Containing Zeolites

	Turnovers[a]	Yields (μmol)[b]		
		epoxide	2-cyclohexen-1-one	2-cyclohexen-1-ol
Fe-FAU	18	2.9	0.7	0.4
$Fe(Me_3tacn)$-FAU	30	3.1	0.7	0.3
$[Fe_2(HPTP)]$-FAU [c]	--	2.0	1.4	0.8
$[Fe_2(HPTP)]$-FAU, oxid.[d]	--	2.6	1.1	0.6
$Fe(HBpz_3)$-FAU [c]	--	2.0	2.1	0.5
$[Fe(H_2O)_6](BF_4)_2$ [e]	0.06	0	0.6	0.37

a-Yield of all oxidation products/mol of iron cations; based on Fe analysis for Fe-FAU and $Fe(Me_3tacn)$-FAU. b-Runs were carried out with 25 mg of faujasite, 80 μmol of cyclohexene, 180 μmol of H_2O_2, in 1.8 mL of CH_3CN, stirred at 25°C for 40 h. Yields were determined by GC and GC/MS. c-These runs were stirred for 20 h. d-This sample had been previously oxidized by exposure to dioxygen. e-In this run, 5.5 mg (1.6×10^{-5} mol) of the ferrous salt was added in place of faujasite.

Since very similar levels of activity are observed in many of the Fe-containing faujasites, the active species in each of these materials may be the same. If this hypothesis is true, then the active center is not bound to an exogenous ligand, since no ligand is present in Fe-FAU and the metal ions do not appear to be bound in oxidized [Fe$_2$(HPTP)]-FAU. This proposal is consistent with the very low loading of iron observed. The various ligands appear to have a limited effect on the product distribution and almost no influence on the level of activity. One possible explanation for these results is that there are two kinds of active sites, one of which produces epoxide whereas the other produces allylic oxidation products. If the negatively charged ligands HPTP and HBpz$_3^-$ allow uptake of a little more iron, and there is a limited quantity of the former sites, then the additional iron would lead to more allylic oxidation. The lack of activity in Fe(PA)-FAU could result from increased local acidity due to the ligand rather than formation of a complex, since complex formation does not appear to block activity in any of the other ligand-containing faujasites.

The production of cyclohexene oxide clearly requires the presence of iron and the zeolite, but there may be another factor in the formation of the allylic oxidation products. In acetonitrile solution, addition of hydrogen peroxide and cyclohexene to [Fe(H$_2$O)$_6$](BF$_4$)$_2$ results in oxidation to iron(III) and the production of small amounts of 2-cyclohexen-1-one and 2-cyclohexen-1-ol. It has been reported previously that iron(II) in rigorously anhydrous acetonitrile solution catalyzes the disproportionation of hydrogen peroxide, but without oxidation of the iron or any oxidation of cyclohexene.[17] The presence of some water in the reagents used in these assays most likely alters the reactivity of the ferrous salt so the products of the reaction resemble those generated in aqueous Fenton chemistry.[17] In the assays with the zeolite catalysts, it is possible that water again plays a role in the allylic oxidations, possibly in conjunction with a

fraction of the iron cations which is not bound to the zeolite lattice. The faujasite does apparently inhibit the disproportionation of hydrogen peroxide catalyzed by free Fe^{2+} in acetonitrile, however, so the presence of unbound cations is not a certainty.

Identity of Active Species. The primary questions about the active center are: 1) What is the oxidation state of iron in the active species, 2) Does the active center contain more than one iron, and 3) What are the active intermediates? None of these questions can be answered conclusively based on what is known at present. Some of the results, however, in conjunction with literature precedents, allow one to make some educated guesses.

The activity of oxidized $[Fe_2(HPTP)]$-FAU suggests that Fe^{3+} is responsible for the oxidation of cyclohexene in this case. Iron(II) in all the reduced Fe-containing faujasites could be oxidized by H_2O_2, resulting in the same iron(III) center produced by O_2 oxidation of $[Fe_2(HPTP)]$-FAU. In addition, exposing a reaction mixture with Fe-FAU to air early in the run did not stop the reaction. These observations point to an iron(III) ion or cluster as the active species, although there is no direct evidence to support this conclusion.

One likely candidate for the active catalyst is an iron in a specific site bound to the lattice of the faujasite. In Fe^{2+}-exchanged Y-zeolite, which has the faujasite structure but a much lower Si/Al ratio than the faujasite in the present study, the iron is believed to occupy specific mononuclear sites associated with the zeolite lattice.[18,19] Mössbauer studies of Y-zeolite samples with Si/Al ratios ranging from 2.5 to 8.9 found that, as aluminum was replaced with silicon, ion-exchanged Fe^{2+} moved towards low-coordinate sites closer to the supercage.[19] The iron atoms in these sites could be reversibly oxidized and reduced with pulses of O_2 (or N_2O) and H_2, and interacted with external nucleophiles such as CO and water. One proposed model suggested that Fe-O-Fe bridges formed upon

oxidation to explain the 2:1 Fe/O stoichiometry observed in oxygen atom uptake,[20] but other models proposed a mononuclear site with one electron provided by a second iron cation.[21]

In the present study it is likely that at least some metal ions in Fe-FAU, and perhaps in some of the other Fe-containing faujasites, occupy sites bound to lattice oxygens. Since the faujasite used in these experiments has a Si/Al ratio of 300, the favored sites are probably low-coordinate and near the supercage, in analogy to the high-silica Y-zeolite (Figure 3.9). One such proposed site, called Site II, is at the center of a hexagonal window (12-atom ring) between supercage and sodalite cage, close to three lattice oxygen atoms.[18] Another possible site in the supercage (Site III') sits among a tetragonal arrangement of oxygen atoms at the intersection of a sodalite cage and a hexagonal prism.[21,22] Water or hydroxide may be bound an iron atom in either of these sites, giving a distorted tetrahedral environment to the metal in Site II (Figure 3.10 A). Since the oxidation state of the active species is not known, one can imagine either Fe^{2+} or Fe^{3+} being present in this site. The proposed Fe-O-Fe oxidized species is not likely to be the active center, since it is more likely to form inside a sodalite cage where the interatomic distances are more favorable but it is inaccessible to substrate.[20] Solvent may have an effect on the stability of iron in any of these sites, freeing ions from the lattice by solvation, and creating ions which are more likely to catalyze allylic oxidation of cyclohexene.

Several non-porphyrin mononuclear iron complexes catalyze the epoxidation of olefins by H_2O_2 in acetonitrile solution.[23-26] Iron(II) complexes of several tetraaza macrocycles, particularly cyclam (1,4,8,11-tetraaza-cyclotetradecane), are among the best, producing only small amounts of allylic oxidation products in up to 20 turnovers.[23,27] Epoxidation of cyclohexene with H_2O_2 is also catalyzed by $FeCl_3$ in acetonitrile and by $Fe(acac)_3$ (acac =

acetylacetonate).[24,25] In addition, there is a diiron(III) complex with mostly carboxylate ligands that also utilizes hydrogen peroxide in the epoxidation of olefins, although with only a few turnovers.[26]

The present system may be analogous to these homogeneous catalysts. A four-coordinate iron cation bound to the lattice could behave as a Lewis acid in a manner similar to the complexes in solution. The reaction occurs more slowly in part because diffusion is slowed in the zeolite, and pores can become blocked by substrate, product, or ligand. A key intermediate proposed for the $Fe(cyclam)^{2+}$ catalyst is a hydroperoxide bound to the iron, stabilized by a hydrogen bond from an axial N-H provided by the ligand.[23] A protonated lattice oxygen could fulfill a similar role in the faujasite. Silicate oxygen atoms are not as likely to bind as tightly to iron as a macrocycle, however, particularly in the presence of solvent with some water. Solvation of metal ions could slow the reaction by removing cations from the primary active site, or promote allylic oxidation by free ions or iron atoms in a different site.

Dinuclear or higher nuclearity species cannot be eliminated as candidates for the active species given what is known at present, although formation of dinuclear complexes seems unlikely at such low levels of iron loading. The effect of such a hydrophobic zeolite on the aggregation of metal ions has not been studied, and it may promote charge neutralization by formation of hydroxo- or oxo-bridged species. Formation of multinuclear metal centers could also provide a plausible reason for why ligand complexes are apparently disfavored, particularly in the oxidized Fe-containing faujasites.

Conclusion

Based on the results obtained so far, it seems that preparation of encapsulated iron complexes can be achieved to a limited extent. The zeolite is not just an inert framework for separating complexes from one another, however. In the absence of ligands, and in some cases even in the presence of ligands, the lattice of the faujasite apparently favors formation of metal centers which can activate hydrogen peroxide for the epoxidation of cyclohexene. A mononuclear iron(III) unit is one likely possiblity for the identity of the active species. One major uncertainty in this work is whether all the iron atoms are contained in a single type of active site or some are present in other sites away from the supercage. Elucidation of these issues will require more detailed study of these materials. In future investigations it is possible that increased activity will be realized by increasing the concentrations of the reagents or by heating the catalyst. In view of the poor conversion of substrate to product at present, such an investigation may not be warranted.

References

(1)   Liu, K. E.; Lippard, S. J. In *Advances in Inorganic Chemistry*; Sykes, A. G., Eds.; Academic Press, Inc.: San Diego, 1995; Vol. 42; pp 263-289.

(2)   Que, L., Jr. In *Iron Carriers and Iron Proteins*; Loehr, T. M., Eds.; VCH: New York, 1989; Vol. 5; pp 467-526.

(3)   Fontecave, M.; Nordlund, P.; Eklund, H.; Reichard, P. In *Advances in Enzymology and Related Areas of Molecular Biology*; Meister, A., Eds.; John Wiley and Sons: New York, 1992; Vol. 65; pp 147-183.

(4)   Bedioui, F. *Coord. Chem. Rev.* **1995**, 44, 39-68.

(5)   Herron, N.; Stucky, G. D.; Tolman, C. A. *J. Chem. Soc., Chem. Commun.* **1986**, 1521.

(6)   Parton, R. F.; Vankelecom, I. F. J.; Casselman, M. J. A.; Bezoukhanova, C. P.; Uytterhoeven, J. B.; Jacobs, P. A. *Nature* **1994**, *370*, 541-544.

(7)   Khouw, C. B.; Li, H. X.; Dartt, C. B.; Davis, M. E. *ACS Symp. Ser.* **1993**, *523*, 273.

(8)   Filatov, M. J.; Pelmenschikov, A. G.; Zhidomirov, G. M. *J. Mol. Catalysis* **1993**, *80*, 243-251.

(9)   Panov, G. I.; Sheveleva, G. A.; Kharitonov, A. S.; Romannikov, V. N.; Vostrikova, L. A. *Applied Catalysis A* **1992**, *82*, 31-36.

(10)   Panov, G. I.; Sobolev, V. I.; Kharitonov, A. S. *J. Mol. Catalysis* **1990**, *61*, 85-97.

(11)   Gaillon, L.; Sajot, N.; Bedioui, F.; Devynck, J.; Balkus, K. J., Jr. *J. Electroanal. Chem.* **1993**, *345*, 157.

(12)   Liu, K. E.; Feig, A. L.; Goldberg, D. P.; Watton, S. P.; Lippard, S. J. In *The Activation of Dioxygen and Homogeneous Catalytic Oxidation*; Barton, D. H. R., Martell, A. E. and Sawyer, D. T., Eds.; Plenum Press: New York, 1993; pp 301-320.

(13)   Feig, A. L.; Becker, M.; Schindler, S.; van Eldik, R.; Lippard, S. J. *Inorg. Chem.* **1996**, *35*, 2590-2601.

(14)   Dong, Y.; Menage, S.; Brennan, B. A.; Elgren, T. E.; Jang, H. G.; Pearce, L. L.; Que, L., Jr. *J. Am. Chem. Soc.* **1993**, *115*, 1851-1859.

(15)   Madison, S. A.; Batal, D. J. International Patent #WO 94/00439. *World Intellectual Property Organization*; 1994.

(16)   Armstrong, W. H.; Spool, A.; Papaefthymiou, G. C.; Frankel, R. B.; Lippard, S. J. *J. Am. Chem. Soc.* **1984**, *106*, 3653-3667.

(17)   Sugimoto, H.; Sawyer, D. T. *J. Am. Chem. Soc.* **1984**, *106*, 4283-4285.

(18)   Delgass, W. N.; Garten, R. L.; Boudart, M. *J. Phys. Chem.* **1969**, *73*, 2970.

(19)   Aparicio, L. M.; Dumesic, J. A.; Fang, S.-M.; Long, M. A.; Ulla, M. A.; Millman, W. S.; Hall, W. K. *J. Catal.* **1987**, *104*, 381-395.

(20)   Garten, R. L.; Delgass, W. N.; Boudart, M. *J. Catal.* **1970**, *18*, 90.

(21)   Segawa, K.; Chen, Y.; Kubsh, J. E.; Delgass, W. N.; Dumesic, J. A.; Hall, W. K. *J. Catal.* **1982**, *76*, 112.

(22)   Mortier, W. J.; Bosmans, H. J. *J. Phys. Chem.* **1971**, *75*, 3327-3334.

(23)   Nam, W.; Ho, R.; Valentine, J. S. *J. Am. Chem. Soc.* **1991**, *113*, 7052-7054.

(24)   Sugimoto, H.; Sawyer, D. T. *J. Org. Chem.* **1985**, *50*, 1784-1786.

(25)   Yamamoto, T.; Kimura, M. *J. Chem. Soc., Chem. Commun.* **1977**, 948-949.

(26)   Murch, B. P.; Bradley, F. C.; Que, L., Jr. *J. Am. Chem. Soc.* **1986**, *108*, 5027-5028.

(27)   Valentine, J. S.; Nam, W.; Ho, R. Y. N. In *The Activation of Dioxygen and Homogeneous Catalytic Oxidation*; Barton, D. H. R., Martell, A. E. and Sawyer, D. T., Eds.; Plenum Press: New York, 1993; pp 183-198.
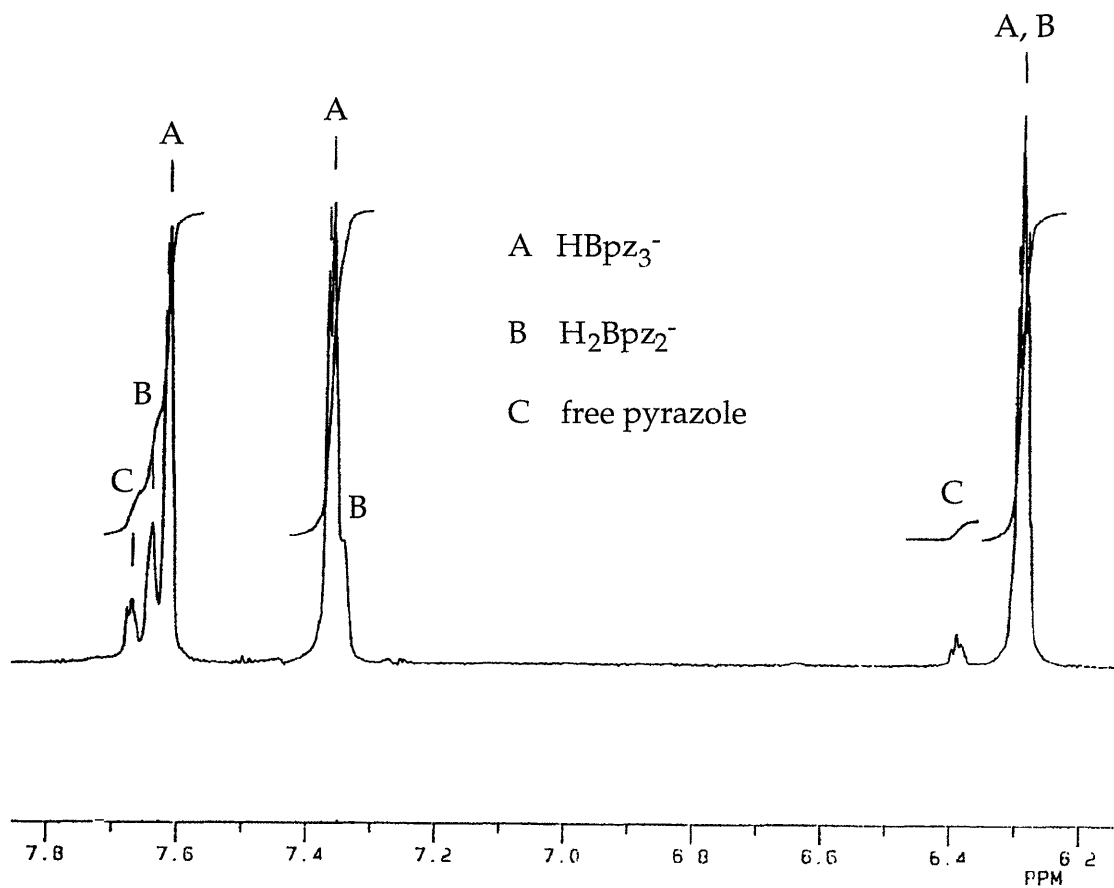
**Figure 3.3:** ^{1}H-NMR spectrum of excess ligand from impregnation of faujasite with KHBpz$_3$.
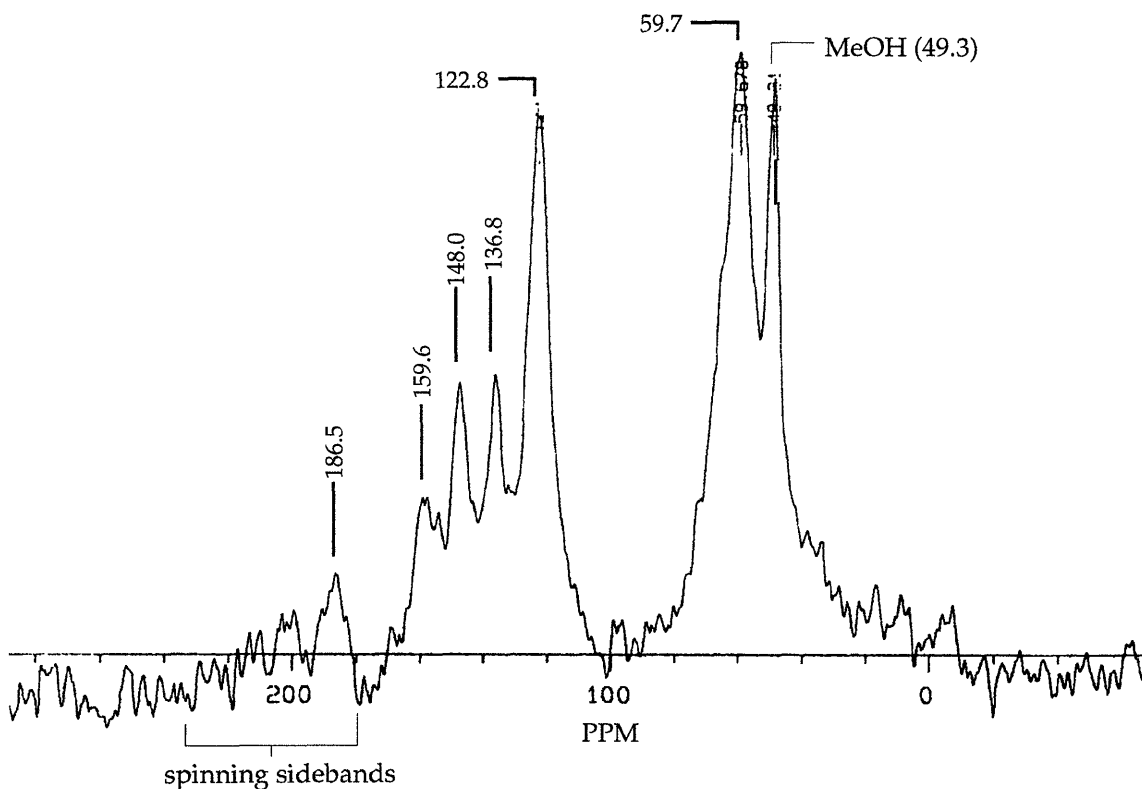
**Figure 3.4:** CPMAS-NMR spectrum of HPTP-FAU (2000 transients, spinning at 4.7 kHz).

Table 3.2: Summary of ^{13}C Chemical Shifts of Ligands in Faujasite and in Solution

| Ligand	ppm in FAU	ppm in CDCl$_3$ [a]
HPTP	59.7	59.3, 60.9, 67.4
	122.8	122.0, 123.2
	136.8	136.5
	148.0	149.0
	159.6	159.6
Me$_3$tacn	45.1	46.7
	52.2	57.1
KHBpz$_3$ [b]	---	105.0
	---	134.7
	---	140.8

a - A linewidth of 500 Hz (~ 7 ppm) in these solid state NMR spectra results in poor resolution of closely spaced peaks. Peaks present in the solution ^{13}C-NMR spectrum are grouped opposite the broad peak in the solid state spectrum which includes the same signals. b - The solution NMR spectrum of KHBpz$_3$ was obtained in CD$_3$OD.

A)

52.2 ———┐   ┌─── 45.1

CH₃OH (49.9) ———┐

B)

66.8

49.934

45.2

Me₃tacn

33.1

14.3

200   100   PPM   0
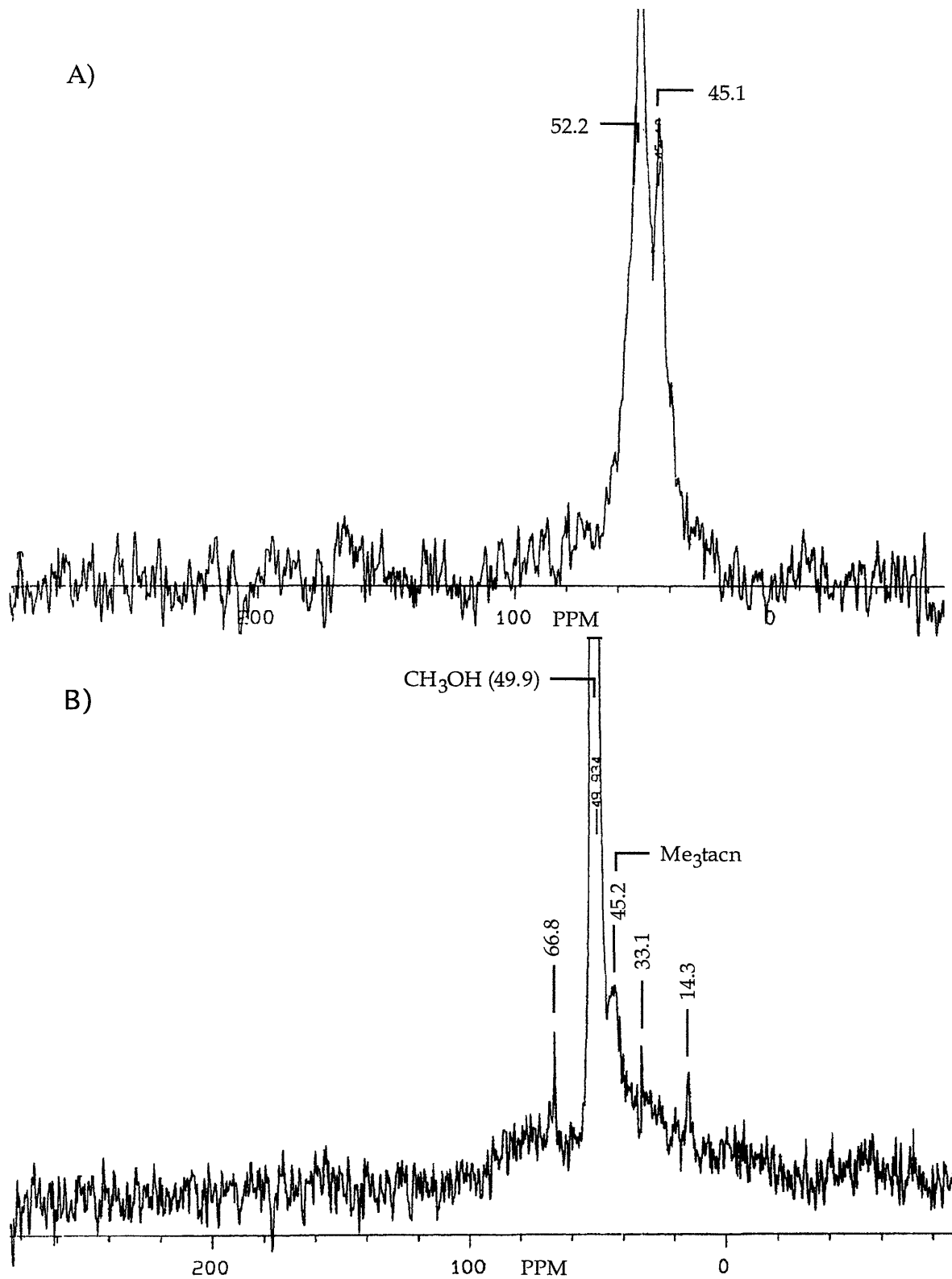
Figure 3.5: CPMAS-NMR spectra of A) Me₃tacn-FAU (800 transients, spinning at 4.7 kHz), and B) Fe(Me₃tacn)-FAU (10,500 transients, spinning at 6.6kHz).
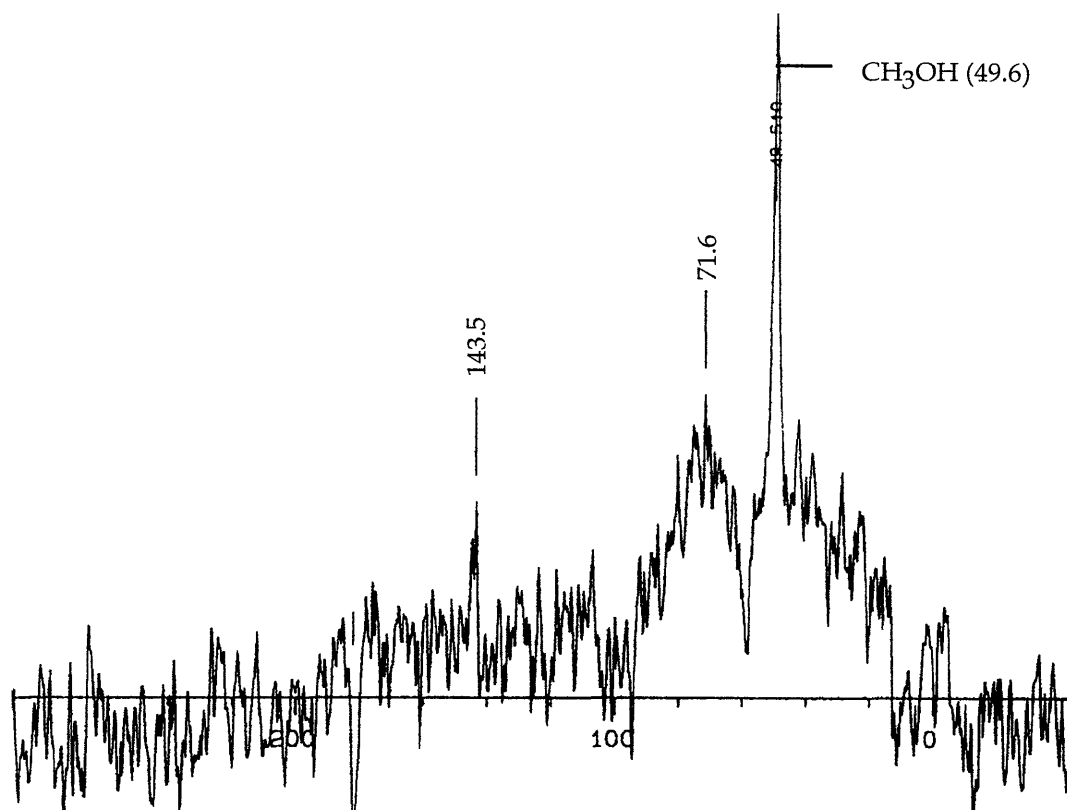
Figure 3.6: CPMAS-NMR spectrum of KHBpz$_3$-FAU (10,500 transients, spinning at 5.2 kHz).
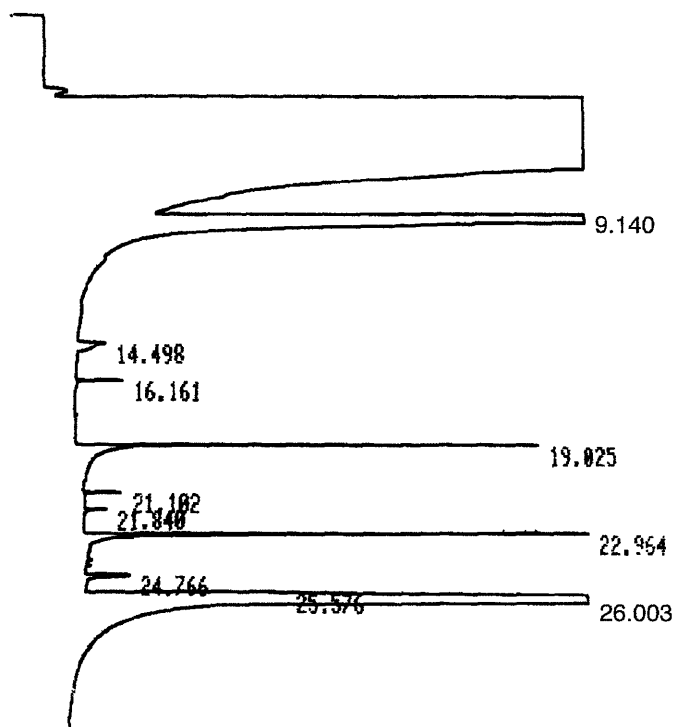
Figure 3.7: GC trace of the reaction mixture from exposure of Fe-FAU to O_2 in the presence of cyclohexene and hydroquinone. The GC conditions used in this experiment are as follows: initial temp., 45°C; initial time, 13 min; heating rate, 15°C/min; final temp., 180°C. The retention times of the important components, both observed and unobserved, are given below.

| Compound	Retention Time (min)
cyclohexene	9.1
cyclohexene oxide	18.1
2-cyclohexene-1-ol	18.9
p-benzoquinone	19.0
2-cyclohexen-1-one	19.7
methyl benzoate (standard)	23.0
hydroquinone	26.0

All the smaller peaks that appear in the GC/MS trace were identified as either solvent impurities (e.g. toluene at 16.16 min) or decomposed column packing material (i.e., oligomethylsiloxanes at 21-22 min).
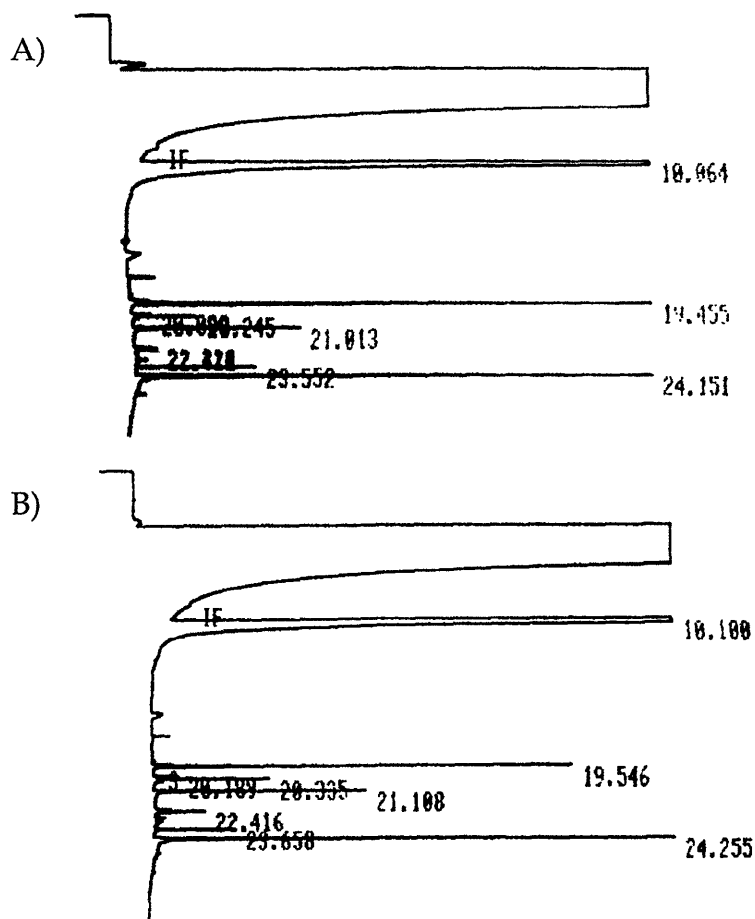
Figure 3.8: GC traces of the reaction mixtures from assays for the oxidation of cyclohexene with H_2O_2 in the presence of A) Fe-FAU and B) previously oxidized [Fe_2(HPTP)]-FAU. The GC conditions used in these experiments are as follows: initial temp., 40°C; initial time, 14 min; heating rate, 15°C/min; final temp., 190°C. The retention times of the major components under these conditions are listed below.

Compound	Retention Time (min)
cyclohexene	10.1
cyclohexene oxide	19.5
2-cyclohexene-1-ol	20.3
2-cyclohexen-1-one	21.1
methyl benzoate (standard)	24.2

The results of these experiments and those involving other Fe-containing faujasites are summarized in Table 3.1.
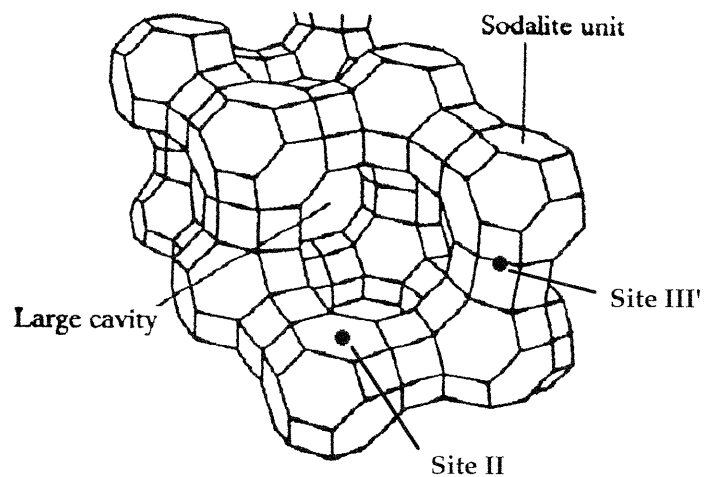
Figure 3.9: Locations of possible mononuclear iron sites in the lattice of the faujasite. Each segment in the structure represents a Si-O-Si(Al) linkage. Site III', which is in the supercage, sits above an oxygen atom which points into the sodalite cage.

A)

Fe

Si/Al

O

H

B)

O atom pointing away from supercage

O atom pointing towards supercage

Si or Al atom

Site III' in the supercage
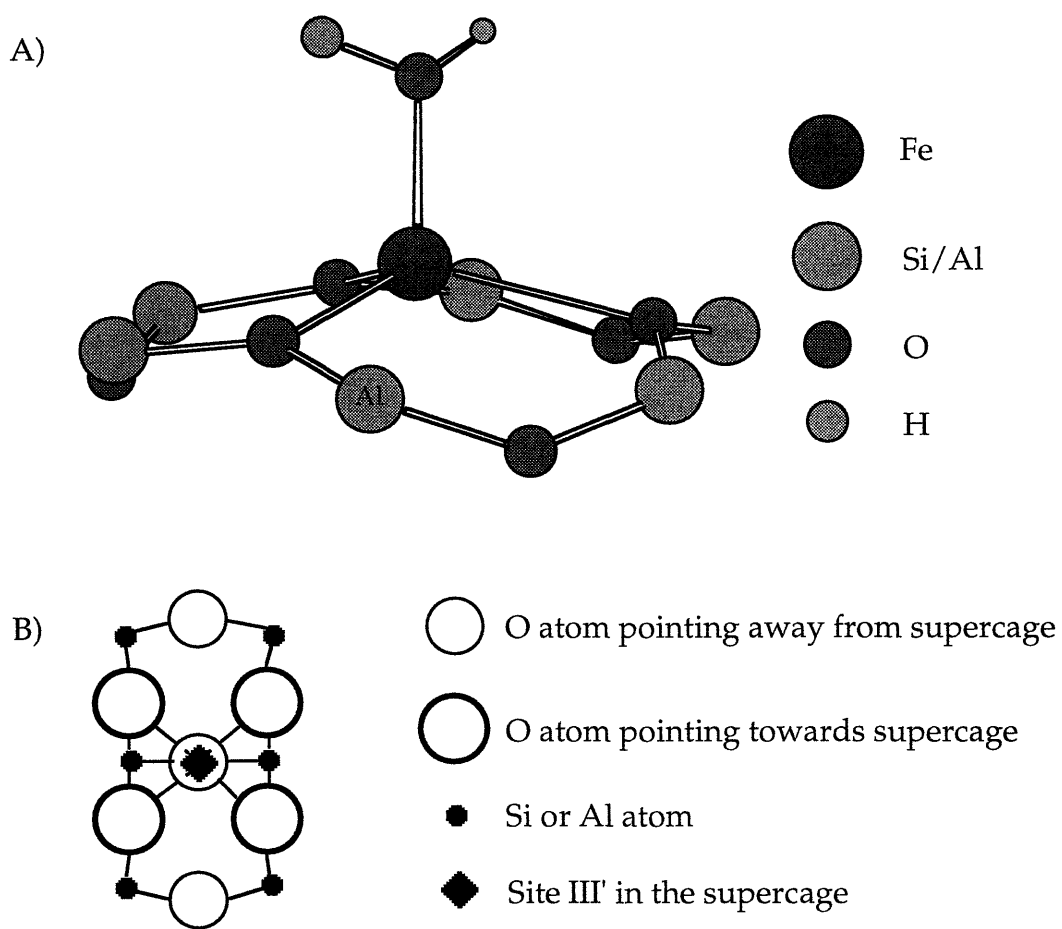
Figure 3.10: A) A Chem3D® representation of the proposed structure of an Fe^{2+} bound at Site II with a coordinated water molecule. B) Diagram of the local environment at Site III'.